

## 6. SITE 1012<sup>1</sup>

### Shipboard Scientific Party<sup>2</sup>

#### HOLE 1012A

**Date occupied:** 3 May 1996  
**Date departed:** 4 May 1996  
**Time on hole:** 1 day, 06 hr, 30 min  
**Position:** 32°16.970'N, 118°23.024'W  
**Drill pipe measurement from rig floor to seafloor (m):** 1784.2  
**Distance between rig floor and sea level (m):** 10.9  
**Water depth (drill pipe measurement from sea level, m):** 1773.3  
**Total depth (from rig floor, m):** 2057.7  
**Penetration (m):** 273.5  
**Number of cores (including cores having no recovery):** 30  
**Total length of cored section (m):** 273.5  
**Total core recovered (m):** 269.7  
**Core recovery (%):** 98.0  
**Oldest sediment cored:**  
Depth (mbsf): 273.50  
Nature: Nannofossil chalk, clay with carbonate  
Age: late Miocene  
**Measured velocity (km/s):** 1.56 at Section 5H-5, 90–93 cm

#### HOLE 1012B

**Date occupied:** 4 May 1996  
**Date departed:** 5 May 1996  
**Time on hole:** 09 hr, 45 min  
**Position:** 32°16.956'N, 118°23.030'W  
**Drill pipe measurement from rig floor to seafloor (m):** 1782.7  
**Distance between rig floor and sea level (m):** 11.0  
**Water depth (drill pipe measurement from sea level, m):** 1771.7  
**Total depth (from rig floor, m):** 1915.0  
**Penetration (m):** 132.3  
**Number of cores (including cores having no recovery):** 14  
**Total length of cored section (m):** 132.3  
**Total core recovered (m):** 131.3  
**Core recovery (%):** 99.0  
**Oldest sediment cored:**  
Depth (mbsf): 132.30  
Nature: Clay with carbonate, nannofossil chalk with clay  
Age: late Pliocene

#### HOLE 1012C

**Date occupied:** 5 May 1996  
**Date departed:** 5 May 1996  
**Time on hole:** 09 hr, 30 min  
**Position:** 32°16.970'N, 118°23.039'W  
**Drill pipe measurement from rig floor to seafloor (m):** 1782.9  
**Distance between rig floor and sea level (m):** 11.0  
**Water depth (drill pipe measurement from sea level, m):** 1771.9  
**Total depth (from rig floor, m):** 1865.5  
**Penetration (m):** 82.6  
**Number of cores (including cores having no recovery):** 9  
**Total length of cored section (m):** 82.6  
**Total core recovered (m):** 86.9  
**Core recovery (%):** 105.0  
**Oldest sediment cored:**  
Depth (mbsf): 82.60  
Nature: Foraminifer nannofossil ooze and calcareous clay mixed sediment  
Age: Pleistocene

**Principal results:** Site 1012 is located in East Cortes Basin, within the middle band of California Borderland basins at a water depth of 1783 m. The primary objective at this site was to sample a high-resolution section from the early Pliocene to Quaternary to study the evolution of the California Current system and oceanographic processes in intermediate waters as Northern Hemisphere glaciations expanded. Paleoceanographic proxies for surface water properties will be obtained at high resolution, including samples for sea-surface temperature, paleoproductivity, and water mass. The site will also be important for high-resolution paleomagnetic studies and will provide important information about organic carbon diagenesis and about minor element geochemistry through interstitial water profiles and geochemical analyses of sediments.

Three holes were cored with the APC/XCB at Site 1012 to a maximum depth of 273.5 mbsf, which recovered uppermost Miocene to Quaternary sediments (Fig. 1). Hole 1012A was cored with the APC to 118.7 mbsf and extended with the XCB to 273.5 mbsf. Hole 1012B was cored with the APC from 0 to 132.3 mbsf and Hole 1012C from 0 to 82.6 mbsf. Detailed comparisons of the three holes between the magnetic susceptibility generated on the MST, and high-resolution color reflectance measured with the Oregon State University system, demonstrated complete recovery of the sedimentary sequence down to 94 mbsf.

The sedimentary section consists of interbedded silty clay, nannofossil mixed sediment, nannofossil ooze, and their lithified equivalents. Volcanic ashes occur infrequently in the upper and lower parts of the sedimentary sequence. The sediments are organic rich and a cyclic variation of organic matter content is superimposed upon the carbonate/siliciclastic cycles. The mean carbonate composition increases downward within the upper 115 mbsf from 15% to 50%. Below 115 mbsf, the carbonate values remain approximately at 50%, although bed-to-bed variation is great. Organic carbon contents are high throughout the sediment column and dominated by marine organic matter. Episodic input of terrigenous organic matter leads to increased organic carbon values. Dolostone beds and the

<sup>1</sup>Lyle, M., Koizumi, I., Richter, C., et al., 1997. *Proc. ODP, Init. Repts.*, 167: College Station, TX (Ocean Drilling Program).

<sup>2</sup>Shipboard Scientific Party is given in the list preceding the Table of Contents.

presence of glauconite are associated with an upper Miocene to upper lower Pliocene hiatus or condensed interval near the base of the sequence. Sedimentation rates average 65 m/m.y. in the Pleistocene and about 50 m/m.y. in the Pliocene.

Biostratigraphic age control was provided by calcareous nannofossils and planktonic foraminifers for the upper Pliocene and Quaternary (Fig. 1). Extensive reworking of calcareous nannofossils in the upper lower Pliocene and uppermost Miocene made biostratigraphic determinations based on calcareous nannofossils difficult. Radiolarians and diatoms are absent in the sequence except for conspicuous reworked middle Miocene species. Lower upper Pliocene microfossil assemblages indicate relatively warm-temperate conditions that changed in the latest Pliocene to Quaternary to cooler conditions, with major sea-surface temperature changes related to glacial/interglacial oscillations.

Paleomagnetic investigations produced an excellent magnetostratigraphic record down to 130 mbsf (Fig. 1) and allowed the identification of the Brunhes, the Jaramillo, Cobb Mountain, and the Olduvai normal polarity intervals. The interstitial water geochemistry reflects the influence of organic carbon diagenesis by sulfate reduction, biogenic opal dissolution, and possible authigenic mineralization reactions. Nonconservative profiles of calcium and magnesium suggest the importance of localized authigenic mineralization. Downhole temperature measurements yield a thermal gradient of 82°C/km and a heatflow estimate of 74 mW/m<sup>2</sup>.

## BACKGROUND AND OBJECTIVES

### General Description

Site 1012 is located about 100 km west of San Diego, California, in East Cortes Basin, within the second band of basins from the seaward edge of the California Borderland (Fig. 2). Water depth is shallower than at Animal Basin (1773 mbsl), and the sill depth for waters entering the deep basin is also shallower at 1415 mbsl (Emery, 1960). The site was surveyed in detail with the *Maurice Ewing* on cruise EW9504 (Lyle et al., 1995a, 1995b; Fig. 3). Site 1012 is located in the deepest part of East Cortes Basin, in its southeast corner. From the seismic reflection profile (Fig. 3), we noted an upper sedimentary section with relatively few seismic reflections, changing at 320 ms TWT below the seafloor (about 250 m) to a unit consisting of larger numbers of highly reflective layers. Drilling was designed to penetrate into this second unit. All of the sediments basically conform to topography and appear hemipelagic in character. Basement is poorly imaged with the twin 80-in<sup>3</sup> water guns used in the survey, but it is at least twice as deep as the drilled section.

### Site Objectives

Site 1012 was drilled to sample a high-resolution section from the early Pliocene to Quaternary to study the evolution of the California Current system and to study oceanographic processes in intermediate waters as Northern Hemisphere glaciation expanded. Deep water within East Cortes Basin enters primarily from the south, from sills connected to Animal Basin (Site 1011; Emery, 1960). Some flow may also come from West Cortes Basin (Fig. 4). Benthic foraminiferal isotope data at Site 1012 should therefore be conditioned by intermediate waters at the sill depth (1415 mbsl). Because of the high sedimentation rates at this site, it will also prove important for high-resolution paleomagnetic studies, because of the sediments' good magnetic properties, despite the high sedimentation rate. If the paleomagnetic data are of sufficiently high quality, data about tectonic rotation of East Cortes Basin may be collected.

Site 1012 will also provide important new information about organic carbon diagenesis and about minor element geochemistry through interstitial water profiles. The only long profiles that now exist from the California Margin are from DSDP Leg 63. During that leg, only a few samples in the upper 100 m of the sediment column

were sampled at each site, primarily because of difficulties in obtaining pristine samples with rotary cores. New interstitial water sampling at this site, especially within the upper 100 m, will better define organic matter oxidation and the removal of oxidants from the interstitial waters and sediments.

## OPERATIONS

### Transit from Site 1011 to Site 1012

The 69.0-nmi transit from Site 1011 to Site 1012 was accomplished in 5.75 hr at an average speed of 11.5 kt. A 3.5-kHz precision depth recorder (PDR) survey was performed while approaching Site 1012. A Datasonics 354M beacon was dropped on Global Positioning System coordinates at 0800 hr on 3 May.

### Hole 1012A

Hole 1012A was spudded at 1145 hr on 3 May. APC Cores 167-1012A-1H through 13H were taken from 0 to 118.7 mbsf with 105.7% recovery (Table 1; see Table 2 on CD-ROM in the back pocket of this volume for a more detailed coring summary). Oriented cores were obtained starting with Core 167-1012A-3H. XCB Cores 167-1012A-14X through 30X were taken to 273.5 mbsf with 93.2% recovery. Headspace methane concentration increased with increasing depth, but no significant higher molecular weight hydrocarbons other than C<sub>1</sub> and C<sub>2</sub> were observed, indicating that the methane is of biogenic origin and not significant for safety and pollution investigations. The hole was filled with heavy mud at the completion of coring.

### Hole 1012B

Hole 1012B was spudded at 1530 hr on 4 May. APC Cores 167-1012B-1H through 14H were taken from 0 to 132.3 mbsf with 99.2% recovery (Table 1). Adara temperature measurements were taken on cores 4H, 6H, 8H, and 10H (see "Physical Properties" section, this chapter).

### Hole 1012C

Hole 1012C was spudded at 0115 hr on 5 May. APC Cores 167-1012C-1H through 9H were taken down to 82.6 mbsf with 105.2% recovery (Table 1). The drill string was tripped back to the surface and secured for the 3¼-hr transit to Site 1013 by 0945 hr on 5 May.

## LITHOSTRATIGRAPHY

### Introduction

A Quaternary to uppermost Miocene (0.0 to 5.6–6.2 Ma) sedimentary sequence with one significant hiatus or condensed interval near its base was cored at Site 1012. The sequence consists almost entirely of interbedded calcareous-rich and siliciclastic-rich fine-grained sediments (Fig. 5). Calcareous nannofossils dominate the calcareous fraction of the sediments, but foraminifers are present as a minor component of most lithologies. Sand and volcanic ash are very rare, with thin deposits occurring at only a few isolated horizons. The sediments are all relatively organic rich, and cyclic variation in organic matter content is superimposed upon the carbonate/siliciclastic cycles.

The stratigraphic sequence is grouped into a single lithologic unit, with two subunits (Fig. 5), based on visual core descriptions, smear-slide estimates, and carbonate analyses. Unit I consists of moderately bioturbated, gradationally interbedded, fine-grained lithologies with

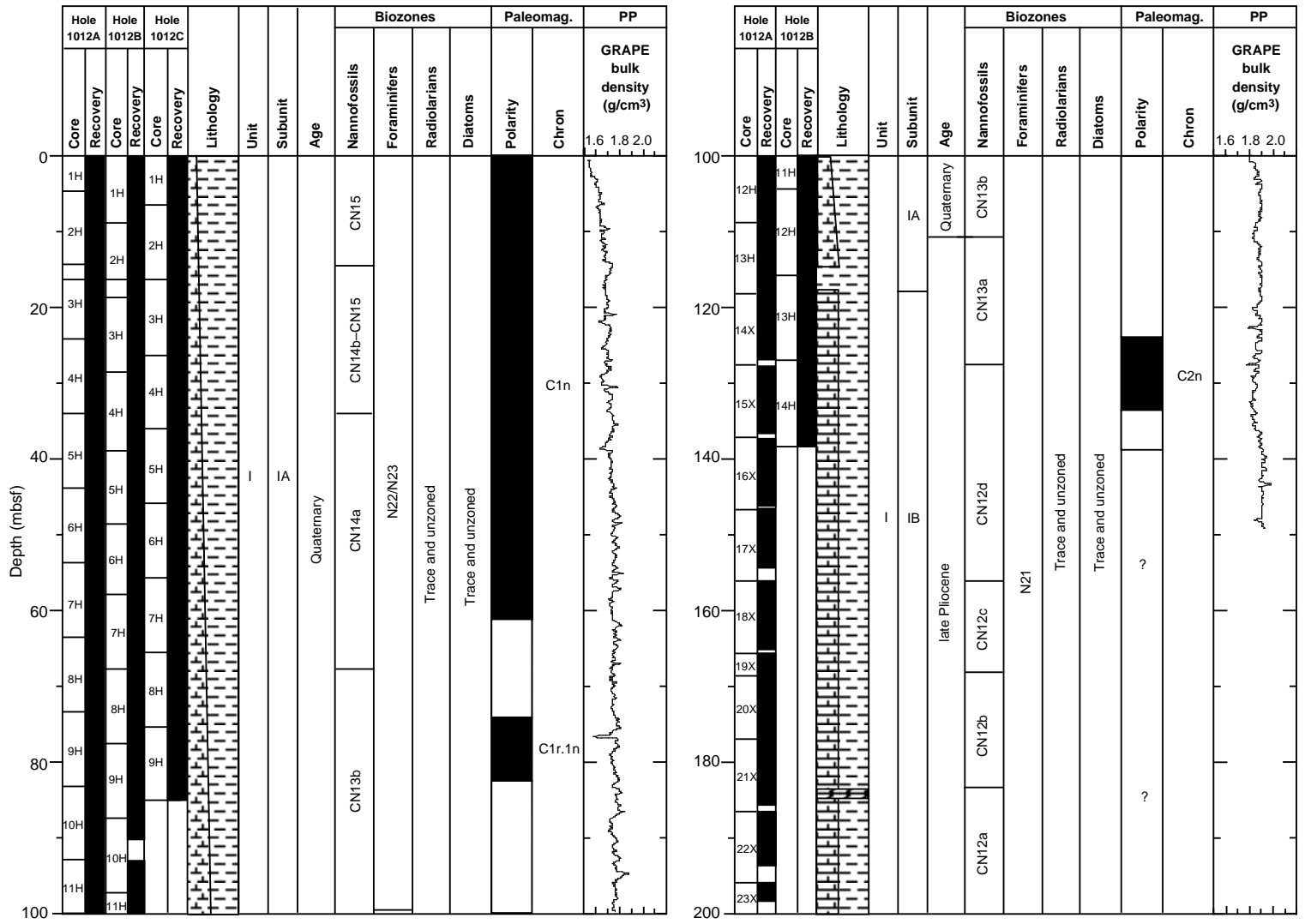


Figure 1. Site 1012 master column.

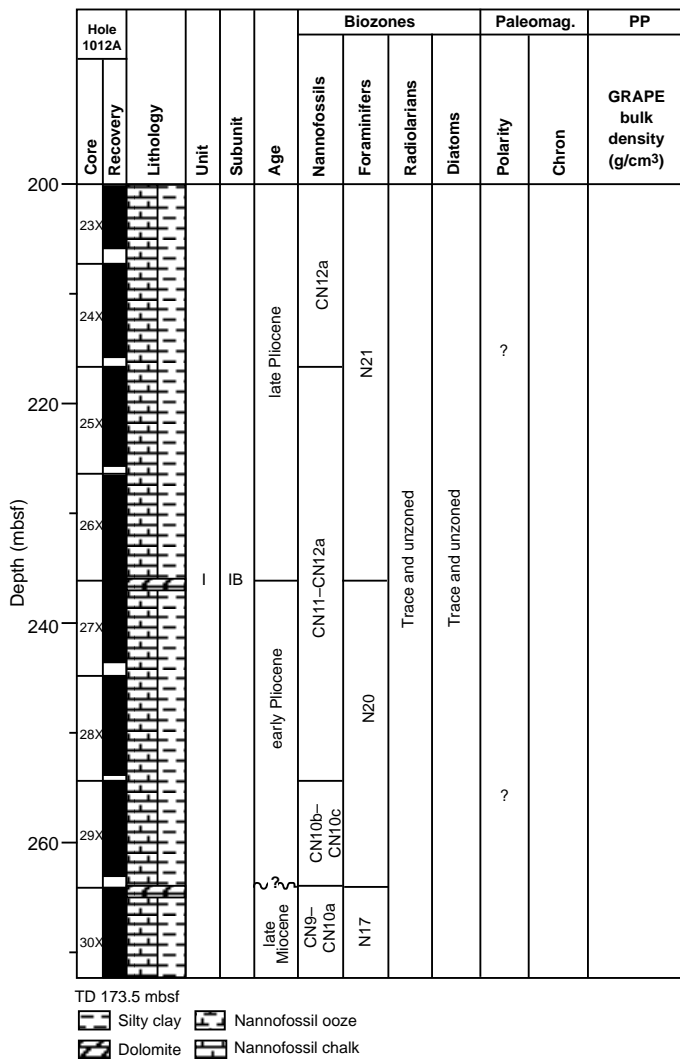


Figure 1 (continued).

varying amounts of calcareous nannofossil and siliciclastic components. The unit is divided into two subunits based on the degree of lithification and the relative abundance of carbonate. Subunit IB is composed of silty clay, clayey nannofossil mixed sediment, and nannofossil chalk, with a few isolated beds of well-indurated dolostone. Organic matter is abundant yet highly variable in quantity throughout much of the two subunits. Contacts between subunits are not strictly defined because of the gradational nature of interbedding in this unit; thus, the 'intervals' given below are only approximate. Subunit IA is composed of silty clay, nannofossil mixed sediment, and nannofossil ooze.

**Description of Units**

**Unit I**

**Subunit IA**

Hole 1012A, interval 167-1012A-1H through 13H-4; 0.0-115.2 mbsf;  
 Hole 1012B, interval 167-1012B-1H through 13H-4; 0.0-115.2 mbsf;  
 Hole 1012C, interval 167-1012C-1H through 9H; 0.0-82.6 mbsf (base of hole).  
 Age: Quaternary to late Pliocene, 0.0-~2.0 Ma.

Subunit IA consists of dark olive gray (5Y 3/2) to dark grayish brown (2.5Y 3/2) silty clay, light to medium olive (10Y 5/2 to 10Y 5/3) nannofossil clay mixed sediment, and light olive gray (5Y 6/2) to pale olive (10Y 5/2) nannofossil ooze, all interbedded on a scale of decimeters to meters. Values of %CaCO<sub>3</sub> vary from <10% to ~90% in individual smear slides, whereas mean %CaCO<sub>3</sub> values monotonically increase from ~15% near the top of the subunit to ~50% near the bottom (see "Inorganic Geochemistry" section, this chapter). Foraminifers contribute 2% to 28% (mean 13%) of the sediment, the bulk of the carbonate being nannofossils. The silt-sized siliciclastic fraction is composed of quartz, feldspar, and volcanic glass, each of which rarely exceed 5%. Pyrite and other opaque minerals form 1% to 3% of most lithologies but are enriched within burrows or in the adjacent sediment (Fig. 6). Sponge spicules and diatoms are present in trace to 2% quantities. Amorphous organic matter content is relatively high (0.5% to 6% by chemical analysis; see "Inorganic Geochemistry" section, this chapter) with large bed-to-bed variations in abundance. Cycles of organic matter enrichment are superimposed on the carbonate/siliciclastic compositional and color oscillations. These cycles are often of the same wavelength but directly out of

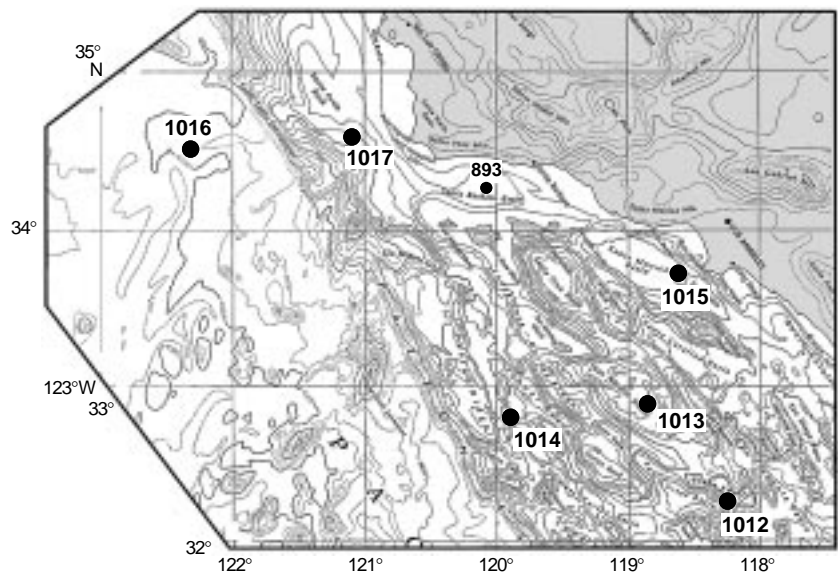


Figure 2. Location map for Site 1012, East Cortes Basin. Site 1012 is located a little more than 100 km southwest of San Diego, California within a basin that probably began to open in the middle Miocene. Other ODP sites are shown for reference.

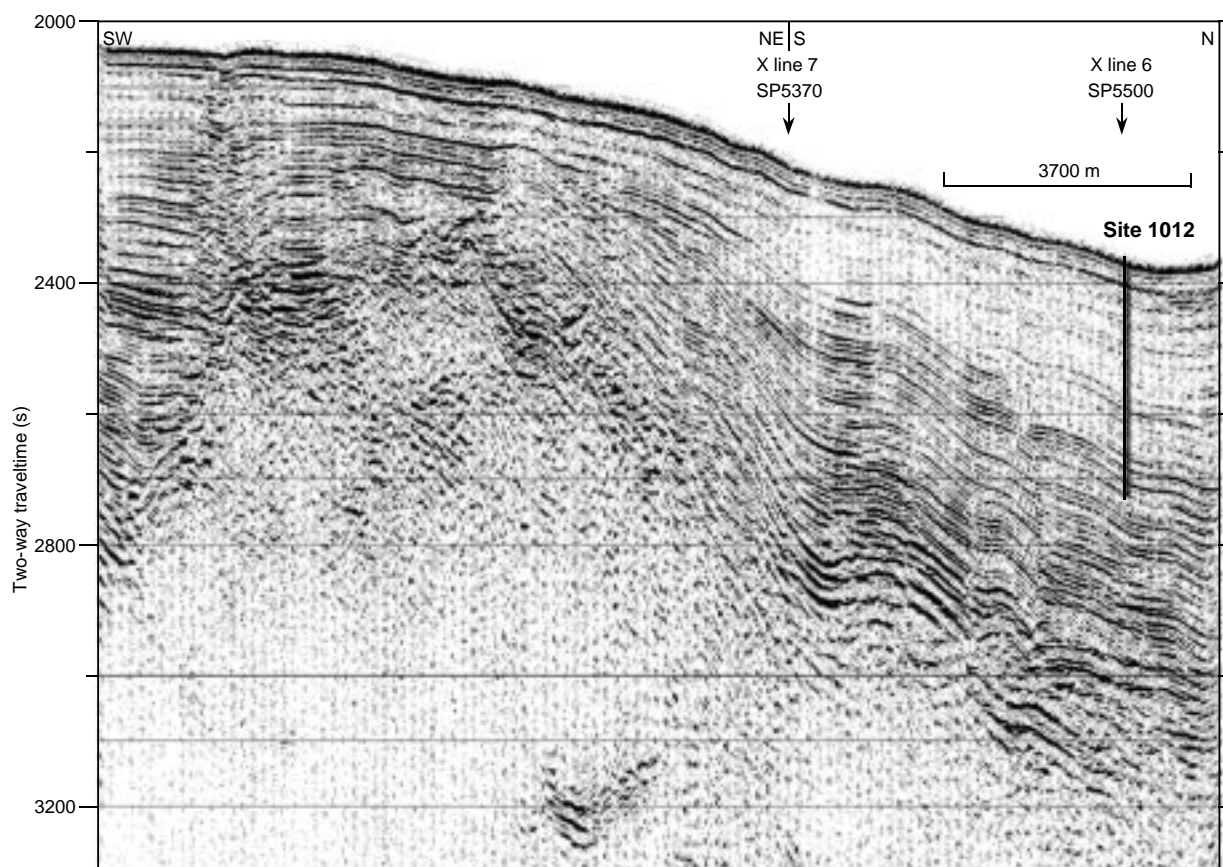


Figure 3. Seismic reflection profile through Site 1012 (EW9504 BA1 Lines 8–10; Lyle et al., 1995a, 1995b). Two prominent seismic units can be identified in the sediment column, an upper transparent unit and a lower, more reflective unit. Basement is poorly imaged but occurs below 3100 ms two-way traveltime (TWT). On y-axis, (s) = milliseconds.

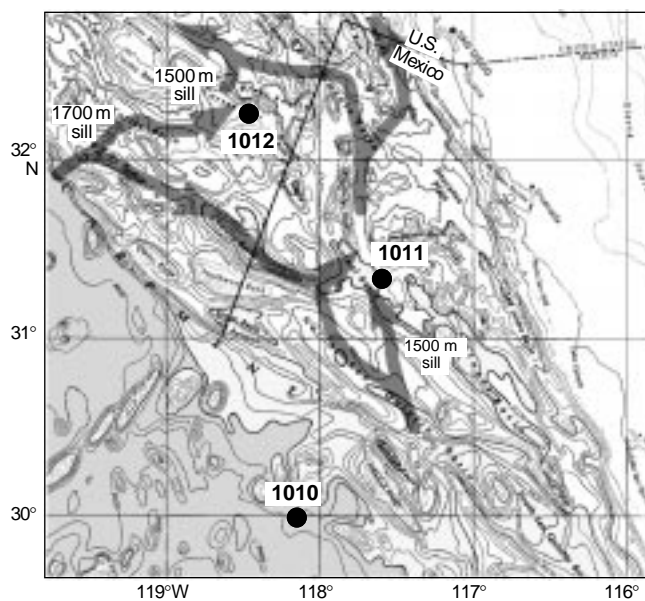


Figure 4. Flow paths for deep water into East Cortes Basin. Emery (1960) suggests that most of the water that flows into the basin comes from the south, from the vicinity of Animal Basin, over a sill of 1415 mbsf.

phase, with organic matter concentration appearing to be inversely proportional to carbonate content. A single, isolated, large pebble of pyritic sandstone with Pholadidae clam borings was found in the midst of nanofossil clay mixed sediment at 132 mbsf. The sediment is mostly homogeneous within individual thick color and compositional bands. Distinct trace fossils are sporadically distributed and only *Chondrites* was identified in this subunit.

#### Subunit IB

Hole 1012A, interval 167-1012A-13H-5 through 30X; 115.2–273.5 mbsf;

Hole 1012B, interval 167-1012B-13H-2 through 14H; 115.2–132.3 mbsf (base of hole).

Age: late Pliocene to latest Miocene, ~2.0 to 5.6–6.2? Ma

The Subunit IA/Subunit IB boundary is gradational and interbedded. The contact is placed at 115 mbsf where the uppermost indurated chalk occurs. This level is closely followed by the depth of APC refusal (119 mbsf). Sediments that were lithified in situ are generally pulverized by XCB coring and thereby artificially rendered soft and plastic. This diagenetic (lithification) horizon is also associated with stabilization of mean total carbonate values at approximately 50% throughout Subunit IB, although bed-to-bed variation remains high (maximum range ~30%).

Subunit IB principally comprises very dark grayish brown (2.5Y 3/2) to olive gray (5Y 4/2) silty clay, dark grayish brown (2.5Y 4/2) to olive gray (5Y 5/2) clayey nanofossil mixed sediment, and light

Table 1. Coring summary for Site 1012.

Core	Date (May 1996)	Time	Top (mbsf)	Bottom (mbsf)	Length cored (m)	Length recovered (m)	Recovery (%)
167-1012A-							
1H	03	1900	0.0	4.7	4.7	4.72	100.0
2H	03	1940	4.7	14.2	9.5	9.94	104.0
3H	03	2020	14.2	23.7	9.5	9.96	105.0
4H	03	2100	23.7	33.2	9.5	9.99	105.0
5H	03	2130	33.2	42.7	9.5	10.13	106.6
6H	03	2200	42.7	52.2	9.5	10.02	105.5
7H	03	2240	52.2	61.7	9.5	10.13	106.6
8H	03	2305	61.7	71.2	9.5	10.09	106.2
9H	03	2340	71.2	80.7	9.5	10.09	106.2
10H	03	0005	80.7	90.2	9.5	9.94	104.0
11H	04	0100	90.2	99.7	9.5	10.18	107.1
12H	04	0135	99.7	109.2	9.5	10.16	106.9
13H	04	0215	109.2	118.7	9.5	10.09	106.2
14X	04	0330	118.7	128.4	9.7	8.94	92.1
15X	04	0425	128.4	138.0	9.6	9.15	95.3
16X	04	0515	138.0	147.6	9.6	9.17	95.5
17X	04	0600	147.6	157.2	9.6	8.72	90.8
18X	04	0650	157.2	166.8	9.6	9.19	95.7
19X	04	0815	166.8	169.9	3.1	3.15	101.0
20X	04	0915	169.9	178.5	8.6	9.54	111.0
21X	04	1015	178.5	188.0	9.5	8.60	90.5
22X	04	1110	188.0	197.6	9.6	7.23	75.3
23X	04	1215	197.6	207.3	9.7	8.36	86.2
24X	04	1300	207.3	216.7	9.4	8.52	90.6
25X	04	1405	216.7	226.4	9.7	8.80	90.7
26X	04	1500	226.4	236.0	9.6	9.69	101.0
27X	04	1645	236.0	244.6	8.6	7.47	86.8
28X	04	1800	244.6	254.2	9.6	9.00	93.7
29X	04	1915	254.2	263.9	9.7	8.69	89.6
30X	04	2030	263.9	273.5	9.6	10.08	105.0
167-1012B-							
1H	04	2245	0.0	8.8	8.8	8.84	100.0
2H	04	2310	8.8	18.3	9.5	9.90	104.0
3H	04	2335	18.3	27.8	9.5	9.90	104.0
4H	05	0030	27.8	37.3	9.5	9.93	104.0
5H	05	0100	37.3	46.8	9.5	9.92	104.0
6H	05	0135	46.8	56.3	9.5	9.98	105.0
7H	05	0217	56.3	65.8	9.5	9.87	104.0
8H	05	0300	65.8	75.3	9.5	10.10	106.3
9H	05	0325	75.3	84.8	9.5	10.09	106.2
10H	05	0400	84.8	94.3	9.5	2.56	26.9
11H	05	0440	94.3	103.8	9.5	9.88	104.0
12H	05	0520	103.8	113.3	9.5	10.15	106.8
13H	05	0545	113.3	122.8	9.5	9.91	104.0
14H	05	0645	122.8	132.3	9.5	10.23	107.7
167-1012C-							
1H	05	0820	0.0	6.6	6.6	6.60	100.0
2H	05	0850	6.6	16.1	9.5	9.88	104.0
3H	05	0915	16.1	25.6	9.5	9.87	104.0
4H	05	0945	25.6	35.1	9.5	10.03	105.6
5H	05	1015	35.1	44.6	9.5	9.98	105.0
6H	05	1040	44.6	54.1	9.5	10.08	106.1
7H	05	1105	54.1	63.6	9.5	10.11	106.4
8H	05	1145	63.6	73.1	9.5	10.18	107.1
9H	05	1220	73.1	82.6	9.5	10.16	106.9

Note: Table 2, on CD-ROM, back pocket, this volume, is a more detailed coring summary.

to medium olive gray (5Y 6/2 to 5Y 5/2) nannofossil chalk. These lithologies are interbedded on a 30–200-cm scale. Composition varies subtly and continuously between the different lithologies. Total carbonate content varies from 25% to 85% (mean 50%), with a lesser contribution from foraminifers than in Subunit IA (0% to 20%, mean 8%). As in the overlying subunit, quartz, feldspar, and volcanic glass make up the silt-size fraction, and pyrite and other opaque minerals are continuously present in trace amounts. Diatoms are present in only trace amounts above 260 mbsf, but form 1% to 3% of most lithologies below, including one bed of diatom nannofossil chalk with nearly 30% diatoms at 245–248 mbsf in Hole 1012A. Three 30- to 50-cm-thick, isolated beds of well-indurated, dark olive gray (5Y 3/2) dolostone occur in the lower half of Subunit IB at 170, 244, and 264 mbsf. Disseminated glauconite is associated with the lowermost of the dolostone beds. The sediment is mostly homogeneous within thick color bands throughout the subunit, and distinct burrows are rare; one cause is the extensive and pervasive sediment disturbance

by XCB coring. Below 244 mbsf, however, *Chondrites* and *Zoophycos* trace fossils are common.

### Depositional History

Sedimentary deposits at Site 1012 record organic-rich hemipelagic sedimentation at a location removed from significant coarse-grained siliciclastic or volcanoclastic input. Deposition is dominated by cyclic alternation between calcareous plankton and terrigenous silt and clay components.

Sediment accumulated slowly (~4–25 m/m.y.) from the latest Miocene to the late early Pliocene (~5.6–6.2 Ma to ~3.7 Ma), possibly including a 1–2 m.y. depositional hiatus (see “Biostratigraphy” section, this chapter). In addition to the silty clay/nannofossil ooze cycles, the condensed stratigraphic interval includes two dolostone beds and disseminated glauconite. Authigenic dolomite and glauconite are frequently associated with reduced sedimentation rates. The con-

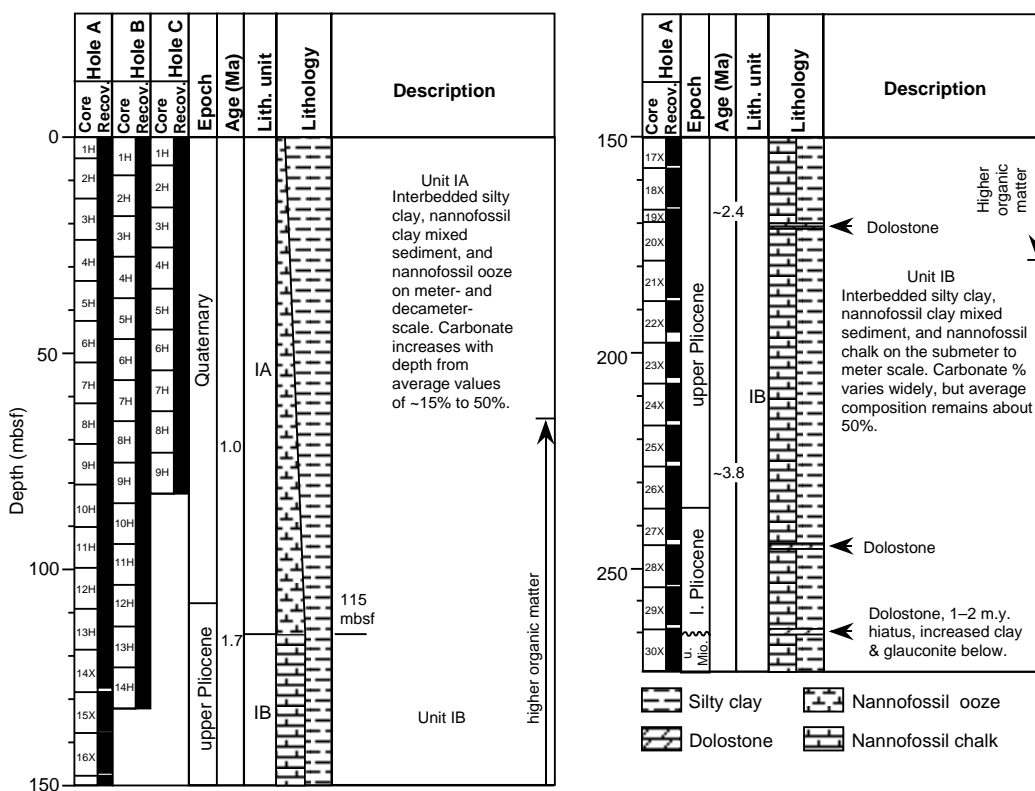


Figure 5. Site 1012 lithostratigraphic summary (0–273.5 mbsf).

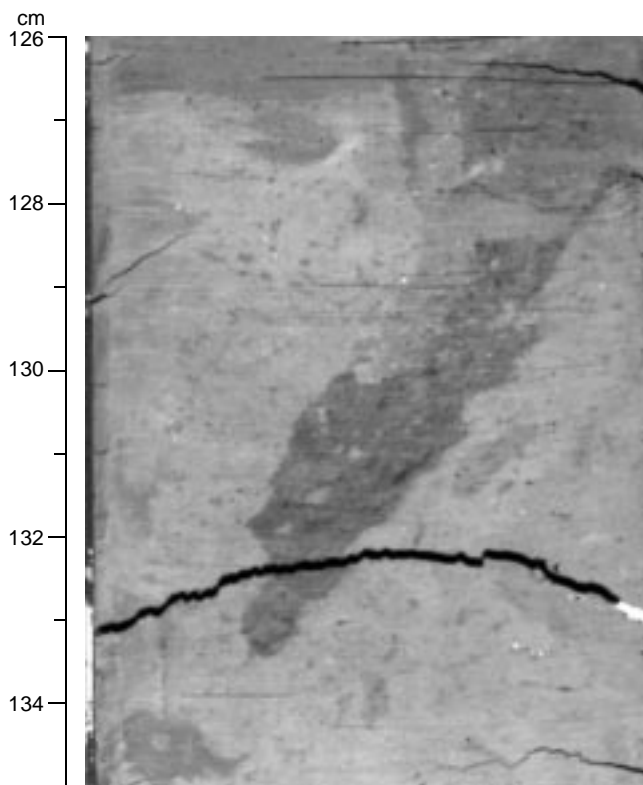


Figure 6. Sediment within burrows are enriched in fine pyrite (Sample 167-1012A-10H-6, 126–135 cm).

Table 3. Depths and datum levels used to place epoch boundaries in Hole 1012A.

Boundary	Depth (mbsf)	Event
Pleistocene/Pliocene	108.34	B <i>G. oceanica</i> s.l.
late/early Pliocene	236	B <i>G. inflata</i>
Pliocene/Miocene	274	T <i>G. conomiozea</i>

Note: B = bottom, T = top.

densified interval documented here approximately corresponds with similar pauses in sedimentation at Sites 1011 and 1014, and may correlate with either the tectonic reorganization of southern and central California between ~5.5–3.4 Ma (McCrorry et al., 1995) or with aspects of the early Pliocene eustatic sea level highstand (Haq et al., 1987).

From the late early Pliocene to the Holocene (~3.7 to 0 Ma) the sedimentation rate accelerated to ~66 m/m.y., with continued cyclic accumulation or dissolution of nannofossil-rich sediments. Carbonate productivity or preservation was enhanced from the late early Pliocene to the Pliocene/Pleistocene boundary (~3.7 to ~1.7 Ma; Subunit IB). From the Pliocene/Pleistocene boundary through the Quaternary (~1.7 to 0 Ma; Subunit IA), the relative carbonate contribution was continuously reduced until nannofossils and foraminifers form only 5%–30% of the total sediment in the late Quaternary.

### BIOSTRATIGRAPHY

The sedimentary sequence recovered from the two holes at Site 1012 consists of an apparently continuous 264-m-thick interval of

**Table 4. Distribution and relative abundances of planktonic foraminifers in Hole 1012A.**

Zone	Core, section, interval	Depth (mbsf)	Abundance	Preservation	<i>Neogloboquadrina dutertrei</i>	<i>Globorotalia tosagensis</i>	<i>Neogloboquadrina humerosa</i>	<i>Globorotalia inflata</i>	<i>Globorotalia punctulata</i>	<i>Globorotalia crassaformis</i>	<i>Neogloboquadrina asanoi</i>	<i>Neogloboquadrina</i> sp. "rounded"	<i>Globigerina</i> cf. <i>druryi</i>	<i>Globorotalia conomiozea</i>	<i>Sphaeroidinella delticensis</i>	<i>Neogloboquadrina pachyderma</i> dex.	<i>Neogloboquadrina pachyderma</i> sin.	<i>Globigerina bullaoides</i>	<i>Orbulina universa</i>	<i>Globigerinoides conglobatus</i>	<i>Globigerinoides ruber</i>	<i>Globorotalia tumida</i>	<i>Globorotaloides hexagona</i>	<i>Sphaeroidinellopsis seminulina</i>	<i>Globigerina woodi</i>	<i>Globorotalia scitula</i>	<i>Globigerinita glutinata</i>	<i>Globigerina quinqueloba</i>	<i>Globigerina umbilicata</i>	<i>Globigerina apertura</i>	<i>Globigerinoides sacculifera</i>		
N22/23	167-1012A-1H-CC	5	A	G	F										A	A	A	C		R					R	R	C	C	C				
	2H-CC	14	A	G	A										A	A	A	C		R					R	R	C	C					
	3H-CC	24	A	G											C	A	A	A	C		R	R		R		R							
	4H-CC	33	A	G	R					R					A	A	A	C		R						R							
	5H-CC	42	A	G	C					R					F	A	A	A	F		R			R									
	6H-CC	52	A	G											A	A	A	A	R		R												
	7H-CC	62	A	G	R										A	A	A	A	F		R					R				R			
	8H-CC	71	A	G											A	A	A	A								R				R			
	9H-CC	81	A	G		C	A	C							A	A	A	A													A		
	10H-CC	90	A	G			A								A																		
	11H-CC	100	A	G				F							A		A	C			F									F			
N21	12H-CC	109	C	G			C	C							C						R												
	13H-CC	119	C	P			A	A	C						A						R												
	14X-CC	128	A	M			A			A					R		A	A	R														
	15X-CC	138	C	M			R	R		R	C				R		A	C															
	16X-CC	147	A	G			A			R	A	A			R	C	A	F	C		F												
	17X-CC	157	C	M			R	R		R	A	A			R	A	A	A	C		F												
	18X-CC	167	A	G			A	R		R	A	A			R	A	A	A	C		F												
	19X-CC	170	A	G			C			R	A	A			R	A	A	A	C		F												
	20X-CC	179	A	G		F	F			R	A	A			R	F	A	C															
	21X-CC	188	A	M						R	A	A			R	C	A	A	C														
	22X-CC	198	A	G			F	F		F	A	A			R	C	C	C			R	R											
	23X-CC	207	A	M			A	C		R	A	A			R	C	A	A	C			R	R										
	24X-CC	217	C	M			I		A	R	A	A			R	A	C	C	F		R	R											
25X-CC	226	F	M			R			R	A	A			R	F	C	C	R			R												
26X-CC	236	A	M			C	A	A	R	A	A			R	F	A	A	F			R												
N19/20	27X-CC	245	B																														
	28X-CC	254	C	G		A				R	A				R					C	R	R	R										
	29X-CC	264	F	M						A	R																						
N17	30X-CC	274	F	G								F	R			R	F	R					R		F						R		

Note: See "Explanatory Notes" chapter for abbreviations.

**Table 5. Coiling dominance of *Neogloboquadrina pachyderma* in latest Pliocene through Quaternary in Hole 1012B.**

Core, section, interval	Depth (mbsf)	<i>Neogloboquadrina pachyderma</i> coiling dominance
167-1012B-1H-CC	5	Sinistral
2H-CC	14	Sinistral
3H-CC	24	Sinistral
4H-CC	42	Sinistral
5H-CC	52	Sinistral
6H-CC	62	Dextral
7H-CC	72	Sinistral
8H-CC	81	Sinistral
9H-CC	90	Sinistral
10H-CC	100	Sinistral
11H-CC	109	Dextral
12H-CC	119	—
13H-CC	128	Sinistral

Note: — = insufficient data to analyze.

upper lower Pliocene to Quaternary sediments. Uppermost Miocene planktonic foraminifers (5.6 to 6.2 Ma) at the bottom of Hole 1012A suggest that much of the lower Pliocene is missing at Site 1012 or that there is a highly condensed lower Pliocene sequence. Calcareous nannofossils are abundant and well preserved in the Quaternary and upper Pliocene, and poorly preserved and fragmented in the upper lower Pliocene and uppermost Miocene. Planktonic foraminifers are highly abundant and very well preserved in the Quaternary, abundant

to common and generally well preserved throughout the Pliocene, and are few but well preserved in the uppermost Miocene. Radiolarians and diatoms are absent in the sequence except for conspicuous reworked middle Miocene species. The entire sequence also records moderate reworking of calcareous nannofossils of middle Miocene age. Planktonic foraminifers show no evidence of major reworking. This suggests that the reworked middle Miocene sediments were rich in diatoms, radiolarians, and calcareous nannofossils but lacked planktonic foraminifers. The base of the sedimentary sequence is assigned to the lowest Pliocene by the presence of *Amaurolithus* spp. and the absence of *Discoaster quinqueramus/berggrenii*. Planktonic foraminifers, however, show the uppermost Miocene based on the presence of *Globorotalia conomiozea*, which indicates an age of ~5.6 to 6.2 Ma.

A well-constrained biostratigraphy and chronology for Hole 1012A is provided by calcareous nannofossils and planktonic foraminifer datums for the upper Pliocene and Quaternary. Extensive reworking of calcareous nannofossils in the upper lower Pliocene and uppermost Miocene made biostratigraphic determinations more difficult based on calcareous nannofossils (Tables 3–6). An age/depth plot for Hole 1012A (Fig. 7) shows an almost continuous sedimentation rate in the sequence from near the base of the upper Pliocene (3.3 Ma) to the Quaternary. A sharp decrease in sedimentation or an unconformity separates the lowest Pliocene to the uppermost Miocene from the upper lower Pliocene. Criteria used for locating epoch boundaries in the sequence are shown in Table 3.

Table 6. Distribution and relative abundances of calcareous nannofossils at Site 1012.

Zone	Core, section, interval (cm)	Depth (mbsf)	Preservation	Abundance	<i>Emilitania huaxleyi</i>	<i>Pseudoemilitania lacunosa</i>	<i>Helicosphaera carteri</i>	<i>Helicosphaera sellii</i>	<i>Gephyrocapsa oceanica</i> s.l.	<i>Gephyrocapsa</i> sp. 3	<i>Gephyrocapsa</i> small	<i>Gephyrocapsa</i> large	<i>Discoaster brouweri</i>	<i>Discoaster triradiatus</i>	<i>Discoaster pentaradiatus</i>	<i>Discoaster surculus</i>	<i>Discoaster tamalis</i>	<i>Discoaster asymmetricus</i>	<i>Reticulofenestra pseudoumbilicus</i>	<i>Reticulofenestra</i> spp.	<i>Ceratholithus rugosus</i>	<i>Ceratholithus</i> spp.	<i>Ceratholithus telesmus</i>	<i>Anaurolithus</i> spp.	<i>Discoaster surculus</i>	<i>Discoaster berggrenii/quinquaramus</i>	<i>Coccolithus pelagicus</i>	<i>Calcidiscus macintyreii</i> >11 µm	<i>Calcidiscus leptopus</i>			
CN15	167-1012A-1H-CC	4.7	G	A	P		C		P		A										R								R			
CN15	2H-CC	14.2	G	C/A	P		C				A																		R			
CN15-CN14b	3H-CC	23.7	P	R			R		P		A																	C	R			
CN15-CN14b	4H-CC	33.2	G	A			R		F		A																			R		
CN14a	5H-CC	42.7	M	C		C	C		R		P											R						R	R			
CN14a	6H-CC	52.2	G	A		C			R	R	P																	C	R	R		
CN14a	7H-CC	61.7	G	A		F	R		R		A																	C	R	R		
CN13b	8H-CC	71.2	M	A		C	R		R																					R		
CN13b	9H-CC	80.7	G	A		C/A	C				P																	RR	F/C	R		
CN13b	10H-CC	90.2	G	A		P			C		P	P																	R	R		
CN13b	11H-CC	99.7	G	A		C		F/C	C		P	P																		F		
CN13b	12H-1, 100	100.7	P	C		C			C		C																			F		
CN13b	12H-2, 105	102.3	M/G	A		C		C	P																					F		
	12H-3, 100	103.7		B																												
CN13b	12H-4, 100	105.2	G	A		C			R																							
CN13b	12H-5, 100	106.7	P	C		C			P																							
CN13b	12H-6, 114	108.3	P	RR					RR																							
CN13b?	12H-7, 45	109.2	G	A		C					C																				C	
CN13b?	12H-CC	109.2	G	A		A					P																				F	
CN13a	13H-CC	118.7	M/G	A		C		R			P		RR																		C/F	
CN13a	14X-CC	128.4	G	A		C		R																							F	
CN12d	15X-CC	138.0	G	A									R																		F	
CN12d	16X-CC	147.6	G/M	A		C		F				R																			C	
CN12d	17X-CC	157.2	P/M	C/A		R						F																			C	
CN12c?	18X-CC	166.8	G	A		C	C	C				F			R																F	
CN12c	19X-CC	169.9	G	A		C	C	C					P	R	F/C																R	
CN12b	20X-CC	178.5	G	A			P						P		F	C															P	
CN12b	21X-CC	188.0	M	A		P							P		F	C															P	
CN12a?	22X-CC	197.6	G	A									P		P	P	R														P	
CN12a	23X-CC	207.3	G	A		P		R					P		C/F	P															P	
CN12a	24X-CC	216.7	M/G	C/A																												P
CN12a-CN11	25X-CC	226.4	M/G	A		F							P																			C
CN12a-CN11	26X-CC	236.0	G	A									P	P																		P
CN12a-CN11	27X-CC	244.6	P	C																												P
CN12a-CN11	28X-CC	254.2	P/M	A																												P
CN10b-CN10c	29X-CC	263.9	P/M	A			C						F																			R
CN10a-CN9	30X-CC	273.5	P	C																												R
	167-1012B-1H-CC	8.8	P	RR			P																									P
	2H-CC	18.3	P	RR			R		P																							R
CN15-CN14b	3H-CC	27.8	G	A			R		C																							R
CN14a	4H-CC	37.3	G	C					R																							R
CN14a	5H-CC	46.8	M/G	A		C	C		R		A																					R

Table 6 (continued).

Zone	Core, section, interval (cm)	Depth (mbsf)	Preservation	Abundance	<i>Emitiantia huxleyi</i>	<i>Pseudoeuammina lacunosa</i>	<i>Helicosphaera carteri</i>	<i>Helicosphaera sellii</i>	<i>Gephyrocapsa</i> sp. 3	<i>Gephyrocapsa</i> small	<i>Gephyrocapsa</i> large	<i>Discosaster brouweri</i>	<i>Discosaster tritadriatus</i>	<i>Discosaster pentaradiatus</i>	<i>Discosaster surculus</i>	<i>Discosaster tamalis</i>	<i>Discosaster asymmetricus</i>	<i>Reticulofenestra</i> spp.	<i>Reticulofenestra pseudombilicus</i>	<i>Reticulofenestra rugosus</i>	<i>Ceratholithus</i> spp.	<i>Ceratholithus telesmus</i>	<i>Ammotithus</i> spp.	<i>Discosaster surculus</i>	<i>Discosaster berggrenii/quintinqueramus</i>	<i>Coccolithus pelagicus</i>	<i>Calcidiscus machinyrei</i> >11 μm	<i>Calcidiscus leptoporus</i>
CN13b	6H-CC	56.3	G	A	C	C	P	R	R	C																		
CN13b?	7H-CC	65.8	G	A	A	A	R		A	A																		
CN13b	8H-CC	75.3	P	F/R	P	P	P		P	P																		
CN13b	9H-CC	84.6	G	A	C	C	P		P	P																		
CN13b	10H-CC	94.3	G	A	C	C	P		P	P																		
CN13b	11H-CC	103.8	M/P	C	F	C	C																					
CN13a	12H-CC	113.3	G	A	C	C	C																					
CN13a	13H-CC	122.8	G/M	C	C	C	C																					
CN13a	14H-CC	132.3	M	A	C	C	C																					

Note: See "Explanatory Notes" chapter for abbreviations.

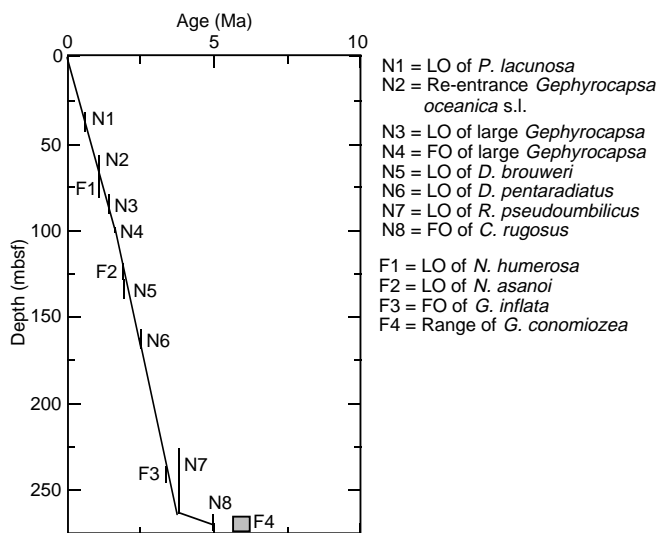


Figure 7. Age/depth plot for Hole 1012B. LO = last occurrence, FO = first occurrence.

A special feature of Site 1012 is the expanded Quaternary sequence (~100 m) containing abundant and well-preserved calcareous microfossils. Early late Pliocene planktonic foraminiferal assemblages indicate relatively warm-temperate conditions. Latest Pliocene to Quaternary planktonic foraminiferal assemblages indicate cooler conditions with major sea-surface temperature changes related to glacial/interglacial oscillations. Conditions were surprisingly cold in the region of Site 1012 during glacial episodes. Benthic foraminifers show no evidence of anoxic or suboxic conditions, but nevertheless reflect relatively low oxygen levels of bottom waters during the Quaternary.

### Planktonic Foraminifers

Site 1012 contains an excellent planktonic foraminifer sequence ranging in age from the latest Miocene (5.6–6.2 Ma) to the Quaternary. The assemblages are highly abundant and very well preserved in the Quaternary and are abundant to common and moderately to well preserved throughout the Pliocene. Specimen fragmentation is pervasive in the Pliocene assemblages, and there tends to be a concentration of robust forms larger than 250 μm. There are few foraminifers in the uppermost Miocene but those present are moderately to well preserved. This report is largely based on observations and tabulation of species in assemblages from core catchers from Hole 1012A (Table 4). Each core-catcher sample from Hole 1012B was examined briefly and the dominance of coiling direction determined in *Neogloboquadrina pachyderma* (Table 5). The biostratigraphy of planktonic foraminifers at Site 1012 is similar to that at Site 1011, except that the Quaternary sequence is much expanded at Site 1012 and thus exhibits faunal changes at a much higher stratigraphic resolution. Site 1012 is of special interest because of the quality of the Quaternary sequence, which is over 100 m thick, contains an abundance of well-preserved planktonic and benthic foraminifers, and clearly records large-scale glacial/interglacial oscillations based on changes in the planktonic foraminifer assemblage composition.

The base of the Quaternary at Site 1012 is not clearly marked because of a paucity of *Globorotalia truncatulinoides* in the sequence, especially in Hole 1012A. In Hole 1012B, the FO of this species occurs at 104 mbsf (Sample 167-1012B-11H-CC) and marks the base of Zone N22. The upper part of the Quaternary (above 62 mbsf; Sample 1012A-7H-CC) is marked by the occurrence of *Neogloboquadrina dutertrei* and an absence of its ancestor *N. humerosa*.

The middle to upper Quaternary is marked by an abundance of sinistrally coiled *N. pachyderma*. The lower part of the Quaternary is marked by the presence of *N. humerosa*. The LO of *N. humerosa* is dated at 1.2 Ma.

A consistent and useful datum occurring within the latest Pliocene Zone N21 at Sites 1010, 1011, and 1012, is the LO of *Neogloboquadrina asanoi*, which is dated at 1.9 Ma. In Hole 1012A, this datum is located at 119 mbsf (Sample 167-1010A-13H-CC). Two additional LOs of biostratigraphic value within Zone N21 are *Globorotalia punctulata* at 167 mbsf (Sample 167-1012A-18X-CC), which is just below the LO of *Neogloboquadrina* sp. (rounded) at 157 mbsf (Sample 167-1012A-17X-CC).

Upper Pliocene assemblages in Sites 1012 and 1011 are distinctive in exhibiting a combination of *Globorotalia inflata*, *N. humerosa*, and *N. asanoi*, and a dominance of dextrally coiled *N. pachyderma*. The lower part of upper Pliocene Zone N21 can be differentiated from the upper part by the occurrence of a primitive rather than advanced form of *G. inflata*. Primitive forms occur from 236 mbsf (Sample 167-1012A-26X-CC) to 167 mbsf (Sample 167-1012A-18X-CC).

The boundary between early and late Pliocene Zones N20 and N21 (between Samples 167-1012A-26X-CC and 167-1012A-27X-CC), is marked by the FOs of *G. inflata* and *Globorotalia crassaformis*. This boundary is dated at 3.3 Ma.

The planktonic foraminiferal assemblages indicate a highly condensed lower Pliocene sequence at Site 1012, from 245 mbsf (Sample 167-1012A-27X-CC) to 264 mbsf (Sample 167-1012A-29X-CC). An early Pliocene age is indicated by the presence of *G. crassaformis* and *N. asanoi* and the absence of *G. inflata*.

The lowest sample examined in Hole 1012A (Sample 167-1012A-30X-CC), at 274 mbsf, contains a well-preserved planktonic foraminifer assemblage of the latest Miocene age, as indicated by the presence of rare *G. conomiozea*, *Globigerina woodi*, and *N. pachyderma* (sinistral), and the absence of Pliocene globorotalids. This assemblage is dominated by *Globigerina bulloides*, perhaps indicating an increase in upwelling.

Planktonic foraminifers, therefore, indicate that much of the early Pliocene is missing in an unconformity or is highly condensed. The presence of glauconite in the latest Miocene sample supports this interpretation. More detailed observations are needed to clarify the biostratigraphy of this interval.

Site 1012 has much potential for the study of paleoceanographic/paleoclimatic history for the interval from 3.3 Ma through the Holocene. The planktonic foraminifer assemblages indicate relative warmth during the latest early Pliocene through late Pliocene (Samples 167-1012A-29X-CC to 17X-CC), cooling during the latest Pliocene through earliest Quaternary (Samples 167-1012A-17C-CC to 10H-CC), and significantly cooler conditions during the remainder of the Quaternary above Samples 167-1012A-10H-CC and 167-1012B-10H-CC. The middle and late Quaternary is dominated by sinistrally coiled *N. pachyderma*.

Benthic foraminifers are abundant, diverse, and extremely well preserved throughout the entire Quaternary at Site 1012. Both delicate and robust forms are abundant. Uvigerinids, buliminids, and *Gyroidina* are consistently present. Bolivinids are persistent but never abundant. The Quaternary assemblages suggest neither low nor high oxygen concentrations in bottom waters throughout this interval. Benthic foraminifers are less abundant, diverse, and well preserved in the Pliocene and uppermost Miocene at Site 1012. Nevertheless, moderately diverse assemblages are present throughout, especially dominated by robust forms. *Uvigerina* persists throughout.

### Calcareous Nannofossils

Nannofossils are generally common to abundant and well preserved through the Quaternary and upper Pliocene in Holes 1012A

and 1012B. In the lower Pliocene the preservation is poor, specimens often are broken, and identification is difficult (Table 6). An interval spanning the upper Miocene/lower Pliocene Zone CN10a–CN9 to the upper Pleistocene Zone CN 15 was recognized in Hole 1012A. Hole 1012B represents an interval ranging from the upper upper Pliocene Zone CN13a to the upper Pleistocene CN15–CN14a.

In the Quaternary, nannofossil assemblages are marked by the presence of *Emiliania huxleyi*, *Pseudoemiliania lacunosa*, *Calcidiscus leptoporus*, *Helicosphaera carteri*, *Helicosphaera sellii*, and several morphotypes of *Gephyrocapsa* spp. and *Ceratolithoides*. The expanded Quaternary sequence allows recognition of most Pleistocene datums.

The Pliocene/Pleistocene boundary is placed at 108.34 mbsf (Sample 167-1012A-12H-6, 114 cm) by the FO of *Gephyrocapsa oceanica* s.l. Pliocene nannofossil assemblages are marked by an association of *Helicosphaera carteri*, *Discoaster brouweri*, *D. tamalis*, *D. pentaradiatus*, *D. surculus*, *Amaurolithus delicatus*, and several morphotypes of *Reticulofenestra* and *Ceratolithus*. The upper/lower Pliocene boundary was recognized between 226.40 mbsf (Sample 167-1012A-25X-CC) and 254.20 mbsf (Sample 167-1012A-28X-CC) by the LO of *Reticulofenestra pseudoumbilicus*, which marks the base of Zone CN12a, but it was difficult to place precisely because of reworking. Presence of *Amaurolithus* spp. and *Ceratolithus* spp. in Sample 167-1012A-29X-CC allows assignment of this interval to the lower Pliocene Zone CN10c/CN10b. The FO of *Ceratolithus rugosus* that occurs between Sample 167-1012A-29X-CC and Sample 167-1012A-30X-CC marks the base of Zone CN10c and the lower Pliocene. In Sample 167-1012A-30X-CC, calcareous nannofossil assemblages are marked by the presence of *Amaurolithus* spp., which indicates lower Pliocene–upper Miocene Zones CN10a and CN9. This suggests a Miocene age but the absence of *Discoaster quinqueramus/berggrenii* (Zone CN9) does not allow certain assignment of latest Miocene for this sample.

### Diatoms

Diatoms are absent to few in the Pliocene and Quaternary at Site 1012. All diatom assemblages are poorly preserved, and neither the Leg 167 north Pacific diatom zonation nor the standard diatom datum levels were recognized in the three holes (Holes 1012A, 1012B, and 1012C).

The poorly preserved assemblages are commonly accompanied by abundant sponge spicules. Large, robust, and fresh biosiliceous skeletons are resistant to dissolution and fragmentation. Diatoms recovered from Site 1012 contain consistent, but typically few, reworked planktonic diatoms from pelagic middle Miocene sediment sequences. These specimens include many diagnostic cool-water taxa such as *Actinocyclus ingens* and *Denticulopsis* spp. (Table 7).

Persistent and scattered common occurrences of reworked specimens as well as numerous sponge spicules indicate strong incursions of marginal shallow waters that are associated with seafloor erosion from Baja California during the latest Cenozoic or from tops of California Borderland ridges.

## PALEOMAGNETISM

### Laboratory Procedures

With the pass-through cryogenic magnetometer, we measured the remanent magnetization of archive halves of 13 APC cores and one XCB core from Hole 1012A, and on 14 APC cores from Hole 1012B. Based on the results after the alternating field (AF) demagnetization at 20 mT, there is an excellent magnetostratigraphic record above 130 mbsf.

The intensity of natural remanent magnetization (NRM) at Holes 1012A and 1012B above 130 mbsf was on the order of 15 mA/m. AF

Table 7. Distribution and relative abundance of diatoms in Holes 1012A and 1012B.

Core, section, interval	Sample depth (mbsf)	Abundance	Preservation	Diatom fragments	<i>Actinocyclus ingens</i>	<i>Actinocyclus ingens nodus</i>	<i>Actinocyclus tsugaruensis</i>	<i>Aulacosira granulata</i>	<i>Coscinodiscus marginatus</i>	<i>Coscinodiscus marginatus fossilis</i>	<i>Coscinodiscus</i> sp.	<i>Crucidentacula nicobarica</i>	<i>Crucidentacula punctata</i>	<i>Denticulopsis dimorpha</i>	<i>Denticulopsis hustedii</i>	<i>Denticulopsis hyalina</i>	<i>Denticulopsis katoyamae</i>	<i>Denticulopsis lauta</i>	<i>Denticulopsis lauta</i> s.l.	<i>Denticulopsis praedimorpha</i>	<i>Neodenticula koizumii</i>	<i>Neodenticula seminiae</i>	<i>Paralia sulcata</i>	<i>Rhizosolenia barboi</i>	<i>Stephanopyxis turris</i>	<i>Stephanopyxis</i> sp.	<i>Synedra jouseana</i>	<i>Thalassionema nitzschioides</i>	<i>Thalassionema nitzschioides parva</i>	<i>Thalassionema robusta</i>	<i>Thalassiosira convexa</i>	<i>Thalassiothrix longissima</i>	Sponge spicules				
167-1012A-1H-CC	4.7	T	P	F					P																										F		
2H-CC	14.2	T	P	F																																	
3H-CC	23.7	R	P						F						P		P		P			T		P										P			
4H-CC	33.2	T	P																																		
5H-CC	42.7	T	P						P																												
6H-CC	52.2	T	P	T																															T		
7H-CC	61.7	T	P												P	P																					
8H-CC	71.2	R	P			P			P						P				P		P																
9H-CC	80.7	T	P																																		
10H-CC	90.2	T	P						P						P																						
11H-CC	99.7	T	P						P												P																
12H-CC	109.2	T	P																																		
13H-CC	118.7	T	P																																		
14X-CC	128.4	B																																			
15X-CC	138.0	T	P			P	P																	P													
16X-CC	147.6	T	P																																		
17X-CC	157.2	T	P						P																												
18X-CC	166.8	T	P						P	P																											
19X-CC	169.9	R	P	F		P	P		P																												
20X-CC	178.5	T	P					P													P																
21X-CC	188.0	T	P																																		
22X-CC	197.6	R	P			P	P		R					P										P			P	P									
23X-CC	207.3	T	P	P																																	
24X-CC	216.7	R	P			P			P				P	P																							
25X-CC	226.4	F	P			P			P					P	P				P																		
26X-CC	236.0	F	P			P			P																												
27X-CC	244.6	T	P																																		
28X-CC	254.2	F	P			P			P						P	P			P	P																	
29X-CC	263.9	T	P	F		P	P		P																												
30X-CC	273.5	T	P						P																												
167-1012B-1H-CC	8.8	T	P						P																												
2H-CC	18.3	T	P			P			P																												
3H-CC	27.8	T	P																																		
4H-CC	37.3	B																																			
5H-CC	46.8	T	P						P										P																		
6H-CC	56.3	T	P						P																												
7H-CC	65.8	T	P												P																						
8H-CC	75.3	T	P												P	P																					
9H-CC	84.8	T	P																																		
10H-CC	94.3	B																																			
11H-CC	103.8	T	P			P																															
12H-CC	113.3	T	P																																		
13H-CC	122.8	T	P						P																												
14H-CC	132.3	T	P			P			P																												

Notes: P = present; more detailed abundance information not available. See "Explanatory Notes" chapter for other abbreviations.

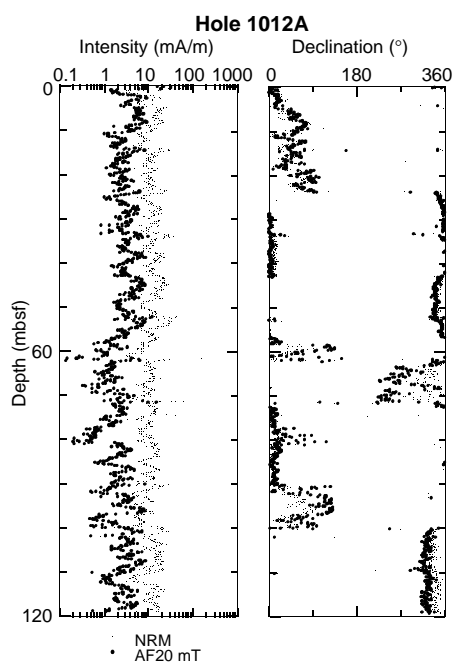


Figure 8. Plots of magnetic intensity (left) and declination (right) of cores from Hole 1012A. Small and large dots represent magnetic intensity before and after AF demagnetization at 20 mT, respectively. There is a strong bias of declination values around 0° because of the radial magnetization overprint, which leads to a magnetization in the x-direction in the archive half of the core.

demagnetization at 20 mT reduced the remanent magnetization to about 25% of its initial value (Fig. 8). When compared with Site 1011, the relative decrease in NRM intensity upon AF demagnetization is less for the cores from Site 1012. This suggests that the carriers of remanent magnetization at Site 1012 have higher remanent coercive forces and smaller grain size than those at Site 1011. Most inclinations after AF demagnetization ranged between 30° and 60°. These inclinations are consistent with the expected value of 52° at a latitude of 32°17' N, assuming a geocentric axial dipole field. We identified normal and reversed polarity chrons based on the polarity of the inclination.

## Results and Discussion

The interpretation of the inclination record after 20 mT AF demagnetization at Holes 1012A and 1012B in terms of geomagnetic polarity chrons is shown in Figure 9. The reversal boundaries with their depths and associated ages are summarized in Table 8. The exact position of a reversal could not be determined at the measurement interval used. A reversal's upper and lower limits are shown in Table 8 as the range in which the reversal is found (typically 10–20 cm). The reversal boundaries in the two holes occur at consistent horizons as correlated by the whole-core magnetic susceptibility measurements (see "Physical Properties" section, this chapter). The presented interpretation of polarity chrons is in agreement with the nannofossil biostratigraphic datums (see "Biostratigraphy" section, this chapter).

Chron C1n (Brunhes) covers the interval from the top of the core to 58.3 mbsf in Hole 1012A. The Jaramillo (C1r.1n) subchronozone occurs over an interval of about 7 m, and its top and bottom are not clearly defined at Hole 1012A. Because of the high sedimentation rate of ~65 m/m.y., even the short Cobb Mountain cryptochron is well resolved from about 83.5 to 85.5 mbsf in Hole 1012A. At 118.5

mbsf there is an indication of the top of a normal magnetozone in Hole 1012A (Fig. 9), which could be assigned to the termination of the Olduvai (C2n).

A comparison of the downhole inclination plots from Holes 1012A and 1012B (Fig. 10) shows strongly similar features in both records. The Brunhes/Matuyama boundary is located at 60.0 mbsf in Hole 1012B, about 2 m deeper than at Hole 1012A, but consistent with the composite depth profile constructed from the MultiSensor Track (MST) data. The onset (bottom) of the Jaramillo is better defined at 82 mbsf in Hole 1012B. The reversed sections at Hole 1012B are not as pronounced as at Hole 1012A, especially in Cores 167-1012B-10H and 11H between 85 and 105 mbsf. We interpret this as being the result of gas expansion disturbing cores and/or a stronger drilling overprint at Hole 1012B, which could not be totally removed with the 20 mT AF. The declinations, even after AF demagnetization at 20 mT, are biased around 0° because of the radial magnetization overprint (Fig. 8). The Olduvai Chronozone was found in Cores 167-1012B-13H and 14H between 120 and 129 mbsf (Fig. 9).

After correlation with the standard polarity time scale (Cande and Kent, 1995) age/depth plots were obtained for Holes 1012A and 1012B (Fig. 11). In the interval from 130 mbsf (about 2 Ma) to the top of the core, the sedimentation rate is constant at approximately 65 m/m.y.

## COMPOSITE DEPTHS AND SEDIMENTATION RATES

Multisensor track (MST) data collected at 4- to 6-cm intervals from Holes 1012A through 1012C, and color reflectance data collected at 6-cm intervals from Holes 1012A and 1012B were used to determine depth offsets in the composite section. On the composite depth scale (expressed as mcd, meters composite depth), features of the plotted MST and color reflectance data present in adjacent holes are aligned so that they occur at approximately the same depth. Working from the top of the sedimentary sequence, a constant was added to the mbsf (meters below seafloor) depth for each core in each hole to arrive at a mcd depth for that core. The depths offsets that compose the composite depth section are given in Table 9 (also on CD-ROM, back pocket). Continuity of the sedimentary sequence was documented only for the upper 90 mcd and between about 116 and 140 mcd. Between 90 and 116 mcd, and below 140 mcd, the cores were placed into composite depth but continuity could not be verified.

Magnetic susceptibility and color reflectance measurements were the primary parameters used for interhole correlation purposes. GRAPE bulk density measurements were not useful for correlations because gas expansion in the cores severely affected the high-resolution bulk density trends. Natural gamma-ray activity measurements were made throughout the entire section in Holes 1012A and 1012B, but the sampling intervals of 12–15 cm were insufficient for correlation.

The magnetic susceptibility and color reflectance records used to verify core overlap for Site 1012 are shown on a composite depth scale in Figures 12 and 13, respectively. The GRAPE data were used to identify voids and intervals of highly disturbed sediments (values less than 1.4 g/cm<sup>3</sup>), and these measurements were culled from all MST data sets (Fig 14). The cores from Holes 1012A, 1012B, and 1012C provide continuous overlap to about 90 mcd. Cores from Holes 1012A and 1012B were placed into composite depth between 90 and 140 mcd, but continuous overlap could not be maintained between 90 and 116 mcd. The composite records suggest that up to 5 m of material may be missing between cores down to about 140 mcd, although the average gap is ~1 m. As there are no data to fill possible core gaps below 140 mcd, an assessment of core gap length below about 140 mcd is not possible.

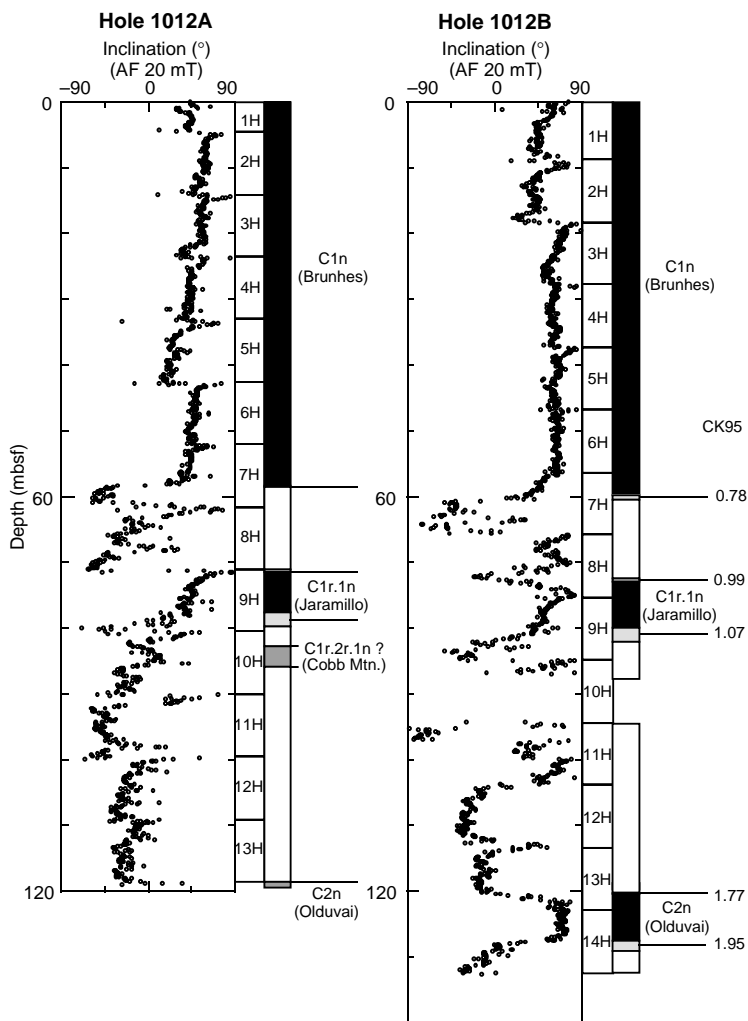


Figure 9. Plots of inclination data from Holes 1012A and 1012B obtained after 20 mT AF demagnetization, with magnetostratigraphic age assignments. Ages from Cande and Kent (1995).

Table 8. Magnetostratigraphic reversal boundaries in Holes 1012A and 1012B.

Chronozone boundary	Age (Ma)	Upper limit			Lower limit		
		Core, section	Level (cm)	Depth (mbsf)	Core, section	Level (cm)	Depth (mbsf)
C1n Brunhes (o)	0.780	167-1012A-7H-5	5	58.25	167-1012A-7H-5	25	58.45
C1r.1n Jaramillo (t)	0.990	8H-7	55	71.25	9H-1	55	71.75
C1r.1n Jaramillo (o)	1.070	9H-5	45	77.65	9H-6	115	79.85
C1r.2r.1n Cobb Mtn. (t)	1.201	10H-2	45	82.65	10H-3	45	84.15
C1r.2r.1n Cobb Mtn. (o)	1.211	10H-4	25	85.45	10H-4	55	85.75
C2n Olduvai (t)	1.770	13H-7	35	118.55	13H-7	65	118.85
C1n Brunhes (o)	0.780	167-1012B-7H-3	125	59.99	167-1012B-7H-4	55	60.75
C1r.1n Jaramillo (t)	0.990	8H-5	75	72.55	8H-5	115	72.95
C1r.1n Jaramillo (o)	1.070	9H-4	125	81.05	9H-5	85	82.15
C2n Olduvai (t)	1.770	13H-5	105	120.35	13H-5	145	120.75
C2n Olduvai (o)	1.950	14H-4	45	127.75	14H-5	55	129.35

Notes: o = onset; t = termination; the assigned ages of the reversal boundaries are according to the time scale of Cande and Kent (1995). The upper and lower limits define the range within which a reversal occurs.

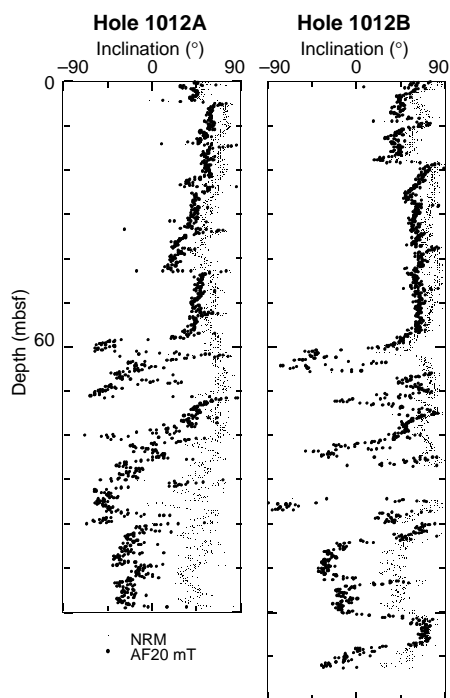


Figure 10. Inclinations before (small dots) and after (large dots) 20 mT AF demagnetization in cores from Holes 1012A and 1012B.

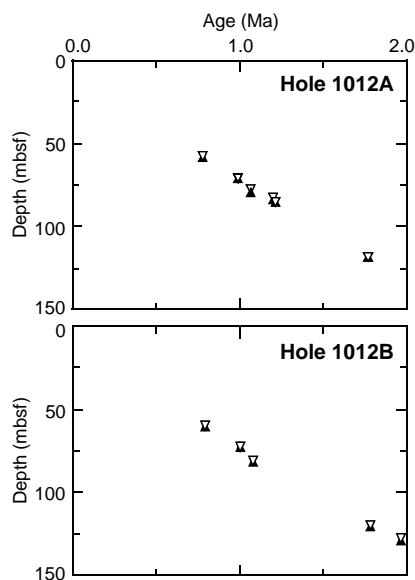


Figure 11. Age/depth plots for Holes 1012A and 1012B. Open and solid triangles show the upper and lower limits of the magnetostratigraphic reversal boundaries.

After constructing the composite depth section for Site 1012, a single spliced record was assembled from the aligned cores. The spliced record consists entirely of Hole 1012A and Hole 1012B cores. Hole 1012B was used as the backbone of the sampling splice. The composite depths were aligned so that tie points between adjacent holes occurred at exactly the same depths in meters composite depth. Intervals having significant disturbance or distortion were avoided if possible. The Site 1012 splice (Table 10, also on CD-ROM, back pocket) can be used as a sampling guide to recover a single continuous sedimentary sequence

Table 9. Site 1012 composite depth section.

Core, section	Depth (mbsf)	Offset (m)	Depth (mcd)
<b>167-1012A-</b>			
1H-1	0	0	0
2H-1	4.7	0.92	5.62
3H-1	14.2	0.86	15.06
4H-1	23.7	1.95	25.65
5H-1	33.2	2.17	35.37
6H-1	42.7	3.15	45.85
7H-1	52.2	3.5	55.7
8H-1	61.7	3.85	65.55
9H-1	71.2	4.43	75.63
10H-1	80.7	5.55	86.25
11H-1	90.2	5.55	95.75
12H-1	99.7	5.87	105.57
13H-1	109.2	5.87	115.07
14X-1	118.7	7.53	126.23
15X-1	128.4	8.41	136.81
16X-1	138	8.41	146.41
17X-1	147.6	8.41	156.01
18X-1	157.2	8.41	165.61
19X-1	166.8	8.41	175.21
20X-1	169.9	8.41	178.31
21X-1	178.5	8.41	186.91
22X-1	188	8.41	196.41
23X-1	197.6	8.41	206.01
24X-1	207.3	8.41	215.71
25X-1	216.7	8.41	225.11
26X-2	227.9	8.41	236.31
27X-1	236	8.41	244.41
28X-1	244.6	8.41	253.01
29X-2	255.43	8.41	263.84
30X-2	264.18	8.41	272.59
<b>167-1012B-</b>			
1H-1	0	0	0
2H-1	8.8	-0.85	7.95
3H-1	18.3	0.33	18.63
4H-1	27.8	1.13	28.93
5H-1	37.3	1.35	38.65
6H-1	46.8	1.62	48.42
7H-1	56.3	1.38	57.68
8H-1	65.8	1.79	67.59
9H-1	75.3	2.43	77.73
10H-1	84.8	3.73	88.53
11H-1	94.3	1.93	96.23
12H-1	103.8	1.93	105.73
13H-1	113.3	4.97	118.27
14H-1	122.8	6.31	129.11
<b>167-1012C-</b>			
1H-1	0	0	0
2H-1	6.6	0.2	6.8
3H-1	16.1	0.69	16.79
4H-1	25.6	1.02	26.62
5H-1	35.1	2.17	37.27
6H-1	44.6	2.64	47.24
7H-1	54.1	3.48	57.58
8H-1	63.6	4.17	67.77
9H-1	73.1	4.53	77.63

Note: This table is also on CD-ROM, back pocket, this volume.

from 0–90 mcd and from 116–140 mcd. For the interval between 95 and 116 mcd, Hole 1012A could not be used to cover core gaps in Hole 1012B, and the spliced record consists of cores appended to each other.

A preliminary age model (Table 11) was constructed to estimate sedimentation rates (Fig. 15). The age model was applied to the spliced records of GRAPE, magnetic susceptibility, and color reflectance shown in Figure 16.

## INORGANIC GEOCHEMISTRY

We collected 14 interstitial water samples from Hole 1012A at depths ranging from 2.95 to 267.13 mbsf. Chemical gradients in the interstitial waters at this site (Table 12) reflect organic matter diagenesis via sulfate reduction, the dissolution of biogenic opal, and the influence of authigenic mineral precipitation.

Chlorinity increases by 1.5% from 2.95 to 18.65 mbsf, then declines to values up to 2% lower than the concentration in the shallowest sample (Fig. 17). Salinity, measured refractively as total dissolved

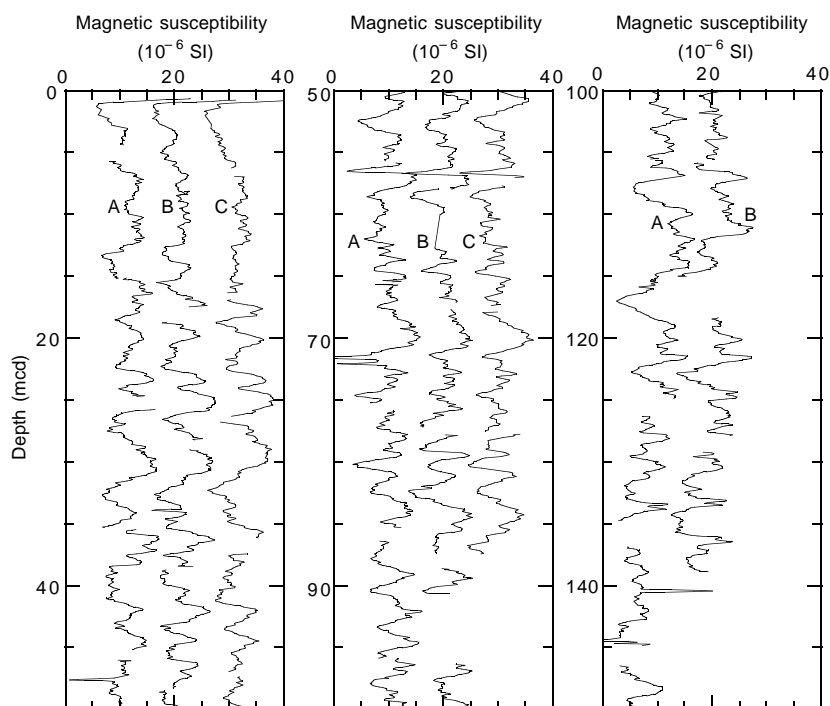


Figure 12. Smoothed (20-cm Gaussian) magnetic susceptibility data for the upper 150 m from Site 1012 on the mcd scale. Holes 1012A through 1012C are offset from each other by a constant ( $10 \times 10^{-6}$  SI).

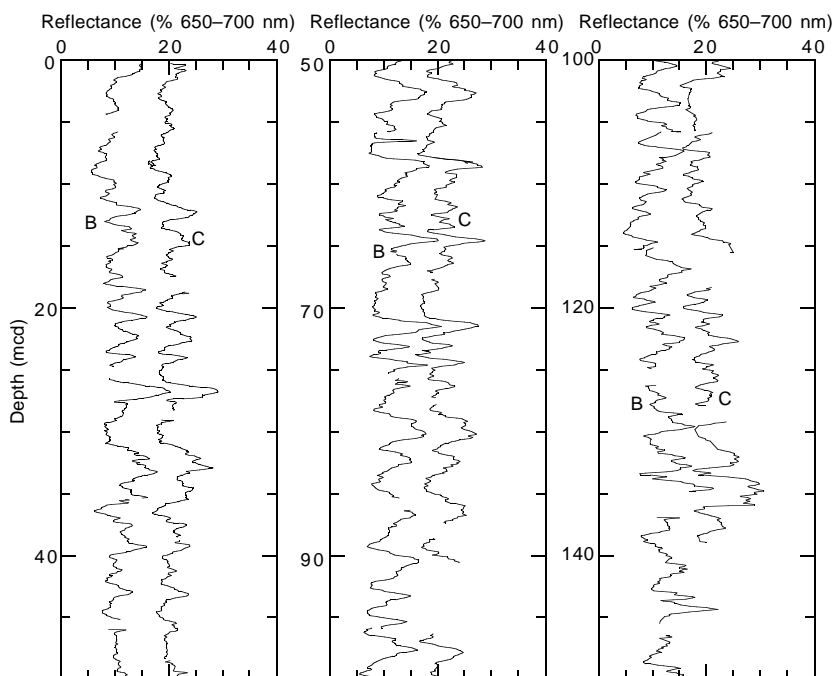


Figure 13. Smoothed (20-cm Gaussian) color reflectance (% 650–700 nm band) data for the upper 150 m from Site 1012 on the mcd scale. Holes 1012B and 1012C are offset from each other by a constant (10%).

solids, generally ranges from 33 to 35. Sodium concentrations measured by flame emission spectrophotometry were on average <0.5% lower than those estimated by charge balance (Table 12).

Alkalinity increases from 4.0 mM at 2.95 mbsf to a peak value of 67.3 mM at 161.75 mbsf (Fig. 17). Sulfate concentrations decrease rapidly in the uppermost sediments to values below the detection limit (~1 mM) by 18.65 mbsf. Phosphate concentrations increase to maximum values of 100  $\mu$ M or greater from 7.45 to 37.65 mbsf, then generally decrease with increasing depth to 16  $\mu$ M in the deepest sample at 267.13 mbsf. Ammonium concentrations increase with increasing

depth to values greater than 14 mM by 131.35 mbsf and persist at these levels downhole. Dissolved manganese concentrations were greater than the detection limit of 3  $\mu$ M only in the shallowest sample, with a concentration of 7.7  $\mu$ M at 2.95 mbsf.

Dissolved silicate concentrations increase with depth to values >1000  $\mu$ M by 131.35 mbsf (Fig. 17), indicative of the dissolution of biogenic opal. Strontium concentrations increase with depth to 343  $\mu$ M at 267.13 mbsf.

Calcium concentrations decrease to values as low as 2.2 mM at 47.22 mbsf, then increase with increasing depth to >6 mM from

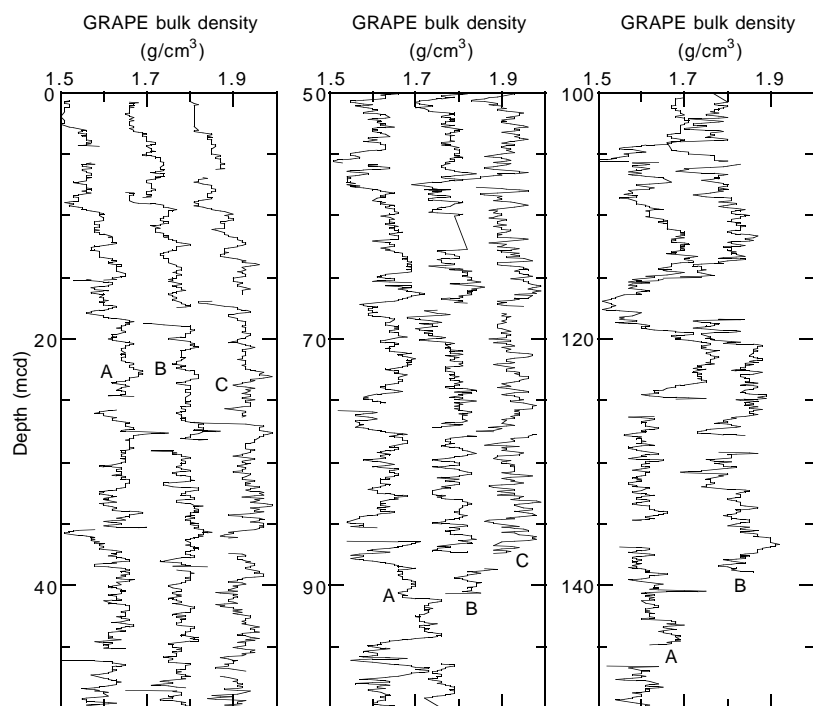


Figure 14. Smoothed (20-cm Gaussian) GRAPE data for the upper 150 m from Site 1012 on the mcd scale. Holes 1012A through 1012C are offset from each other by a constant (0.1 g/cm<sup>3</sup>).

Table 10. Site 1012 splice tie points.

Hole, core, section, interval (cm)	Depth			Hole, core, section, interval (cm)	Depth	
	(mbsf)	mcd			(mbsf)	mcd
1012B-1H-5, 95	6.95	6.95	tie to	1012A-2H-1, 133	6.03	6.95
1012A-2H-4, 107	10.27	11.19	tie to	1012B-2H-3, 24	12.04	11.19
1012B-2H-7, 19	17.99	17.14	tie to	1012A-3H-2, 58	16.28	17.14
1012A-3H-3, 95	18.15	19.01	tie to	1012B-3H-1, 38	18.68	19.01
1012B-3H-6, 63	26.43	26.76	tie to	1012A-4H-1, 111	24.76	26.76
1012A-4H-3, 83	27.53	29.48	tie to	1012B-4H-1, 55	28.35	29.48
1012B-4H-6, 139	36.69	37.82	tie to	1012A-5H-2, 96	35.66	37.82
1012A-5H-3, 79	36.99	39.16	tie to	1012B-5H-1, 51	37.81	39.16
1012B-5H-6, 83	45.63	46.98	tie to	1012A-6H-1, 113	43.83	46.98
1012A-6H-3, 115	46.92	50.07	tie to	1012B-6H-2, 15	48.45	50.07
1012B-6H-6, 139	55.69	57.31	tie to	1012A-7H-2, 11	53.81	57.31
1012A-7H-6, 91	60.61	64.11	tie to	1012B-7H-5, 144	62.73	64.11
1012B-7H-7, 95	65.24	66.62	tie to	1012A-8H-1, 107	62.77	66.62
1012A-8H-2, 131	64.51	68.36	tie to	1012B-8H-1, 77	66.57	68.36
1012B-8H-6, 103	74.33	76.12	tie to	1012A-9H-1, 49	71.69	76.12
1012A-9H-2, 87	73.57	78.00	tie to	1012B-9H-1, 27	75.57	78.00
1012B-9H-6, 123	84.03	86.46	tie to	1012A-10H-1, 21	80.91	86.46
1012A-10H-7, 59	90.29	95.84	tie to	1012B-11H-1, 9	90.28	95.84
1012A-11H-1, 139	91.59	97.14	tie to	1012B-11H-1, 91	95.2	97.14
1012B-11H-7, 39	103.69	105.62	tie to	1012B-11H-7, 36	103.69	105.62
1012B-12H-7, 31	113.11	115.04	tie to	1012A-12H-7, 85	109.17	115.04
1012A-13H-4, 119	114.89	120.76	tie to	1012B-13H-2, 99	115.79	120.76
1012B-13H-7, 35	122.65	127.62	tie to	1012A-14X-1, 139	120.09	127.62
1012A-14X-3, 123	122.93	130.46	tie to	1012B-14H-1, 135	124.15	130.46
1012B-14H-7, 11	131.91	138.22	tie to	1012A-15X-1, 141	129.81	138.22

Note: This table is also on CD-ROM, back pocket, this volume.

Table 11. Site 1012 sedimentation rate age control points.

Event	Chron/ subchron	Depth (mcd)	Age (Ma)
T <i>P. lacunosa</i>		36.90	0.46
B Brunhes	C1n	61.85	0.78
T Jaramillo	C1r.1n	75.95	0.99
B Jaramillo	C1r.1n	83.18	1.07
B Cobb Mountain	C1r.2r.1n	89.75	1.21
B large <i>Gephyrocapsa</i> spp.		103.53	1.44
T Olduvai	C2n	124.57	1.77
T <i>D. brouweri</i>		141.61	1.96
T <i>D. pentaradiatus</i>		170.41	2.50
T <i>R. pseudoumbilicus</i>		253.56	3.79
B <i>C. rugosus</i>		277.11	5.07

Note: T= top; B = bottom.

211.75 to 267.13 mbsf (Fig. 17). Magnesium concentrations decrease to 45.7 mM at 47.22 mbsf, then increase to just over 50 mM from 104.32 to 131.35 mbsf, and then decrease to 36.6 mM at 267.13 mbsf. The decrease in dissolved calcium in the upper sediment and the non-linear relationship of calcium and magnesium suggest that authigenic mineral precipitation is significant in influencing these profiles. Lithium concentrations increase with depth to 268  $\mu$ M at 267.13 mbsf (Fig. 17).

## ORGANIC GEOCHEMISTRY

We conducted measurements of elemental composition and volatile hydrocarbons in sediments from Site 1012 (for methods see "Explanatory Notes" chapter, this volume).

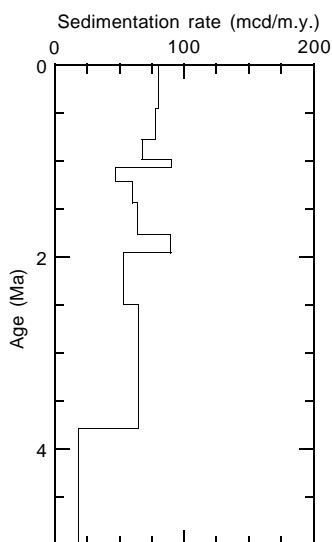


Figure 15. Sedimentation rate vs. age based on the age control points from Table 11.

### Volatile Hydrocarbons

In accord with shipboard safety and pollution prevention considerations, the concentrations of methane, ethane, and propane were routinely monitored at Hole 1012A. The results are displayed in Figure 18 and Table 13. Headspace methane concentration increases rapidly to 12,000 ppm at 20 mbsf. Below ~20 mbsf, the concentration generally decreases with little fluctuation to values of ~4000 ppm. Methane/ethane ratios show a decreasing pattern from top (11,000 ppm) to bottom (700 ppm) of the hole. No significant amounts of higher molecular weight hydrocarbons were observed, indicating that the methane has been derived from biogenic organic matter degradation, and thus is not significant for safety and pollution investigations. Whenever gas voids occurred, vacutainer samples were taken. Because of the direct gas sampling method, the values of the vacutainer samples are higher, but show the same pattern as the headspace samples.

### Elemental Analysis

At Site 1012, 183 sediment samples were analyzed for total carbon, inorganic carbon, total nitrogen, and total sulfur. Results are presented in Table 14 (also on CD-ROM back pocket, this volume) and Figure 19.

The percentage of calcium carbonate ( $\text{CaCO}_3$ ) was calculated from the inorganic carbon concentrations by assuming that all carbonate occurs in the form of calcite. The  $\text{CaCO}_3$  record reflects the overall uniformity of the sedimentary section at this site (see "Lithostratigraphy" section, this chapter). Average values of  $\text{CaCO}_3$  concentration increase with depth in the upper 115 mbsf and stay consistently high (~50 wt%) in the lower part of the core. Within the entire section, carbonate contents show a high fluctuation of ~30 wt%. Only the lowermost 40 mbsf show a lower amplitude variation. This high fluctuation is probably induced by changes in sea-surface productivity rather than dissolution, indicated by very well-preserved calcareous foraminifers and nannofossils in the Quaternary and upper Pliocene sediments (see "Biostratigraphy" section, this chapter).

The organic carbon record is characterized by very high concentrations of ~1–4 wt% throughout the sequence (Table 14; Fig. 19). Some single spikes of up to 6 wt% occur. A high-amplitude variation is visible in the interval between 50 and 180 mbsf. As recognized at

Sites 1010 and 1011, the variation of organic carbon occurs on less than a meter scale, which is also visible in the color of the sediment. Dark greenish intervals display higher organic carbon contents, whereas lighter intervals are carbonate rich and organic-carbon lean.

Total nitrogen values at Site 1012 vary between 0.13 and 0.66 wt%. Total sulfur content ranges from 0 to about 1.73 wt% (Table 14). To characterize the type of organic matter in the sediments, total organic carbon/total nitrogen (TOC/TN) ratios were used. Most of the TOC/TN ratios are below 12, similar to the ratios observed at Site 1011, indicating a predominance of marine organic matter (Fig. 19; Bordovskiy, 1965; Emerson and Hedges, 1988). A slightly positive correlation between total organic carbon and TOC/TN ratio (Fig. 20) indicates that episodic supply of terrigenous organic matter may have resulted in enhanced TOC values.

## PHYSICAL PROPERTIES

### Multisensor Track Measurements

The shipboard physical properties program at Site 1012 included nondestructive measurements of bulk density, magnetic susceptibility, *P*-wave velocity, and natural gamma-ray activity on whole sections of all cores using the MST (Fig. 21). Magnetic susceptibility was measured at 4-cm intervals in Holes 1012A and 1012B and at 6-cm intervals in Hole 1012C at low sensitivity (1-s measuring time). GRAPE bulk density measurements were made at 4-cm intervals in Holes 1012A and 1012B and 6-cm intervals in Hole 1012C. The PWL gave poor velocity results because of signal attenuation and sediment cracking from high gas content (see "Organic Geochemistry" section, this chapter) and was not used for any cores from Hole 1012C. Natural gamma activity was measured with a 10-s count every 15 cm in Holes 1012A and 1012B but was deactivated for Hole 1012C.

### Index Properties

Index properties measurements were made at one sample per working section in the first 21 cores and below this at an average of three per core to total depth (TD) in Hole 1012A. Index properties were determined using gravimetric Method C (see "Explanatory Notes" section, this chapter). Index property data are presented in Table 15 on CD-ROM in the back pocket of this volume. In addition to bulk density, the index properties of void ratio, porosity, water content, dry-bulk density, and grain density were determined (Fig. 22). Calcium carbonate was determined from samples collected adjacent to index properties samples in Hole 1012A and a correlation is seen between calcium carbonate content and bulk density (Fig. 23). There is a downhole increase in both properties (Fig. 24) to APC refusal (148 mbsf), with the scatter reflecting the interbedded  $\text{CaCO}_3$ -rich nannofossil- and foraminifer-rich oozes and  $\text{CaCO}_3$ -poor clays (see "Lithostratigraphy" section, this chapter).

### Compressional-Wave Velocity

One *P*-wave velocity measurement was made in each section in Hole 1012A to a depth of 40 mbsf. At Hole 1012A, the insertable probes of the digital sound velocimeter (pairs T1 and T2) were used for only the first set of measurements (Section 167-1012A-1H-1). Thereafter, in order to avoid the problems associated with added pressure (see "Physical Properties" section, "Site 1011" chapter, this volume), the Hamilton Frame (pair T3) was used exclusively to measure sonic velocity in the *x*-direction (see "Physical Properties" section, "Explanatory Notes" chapter, this volume) while the core was still in the liner in the first five cores (Table 16 on CD-ROM in the back pocket of this volume). Unfortunately, beyond about 40 mbsf the sediments became too gassy (see "Organic Geochemistry" sec-

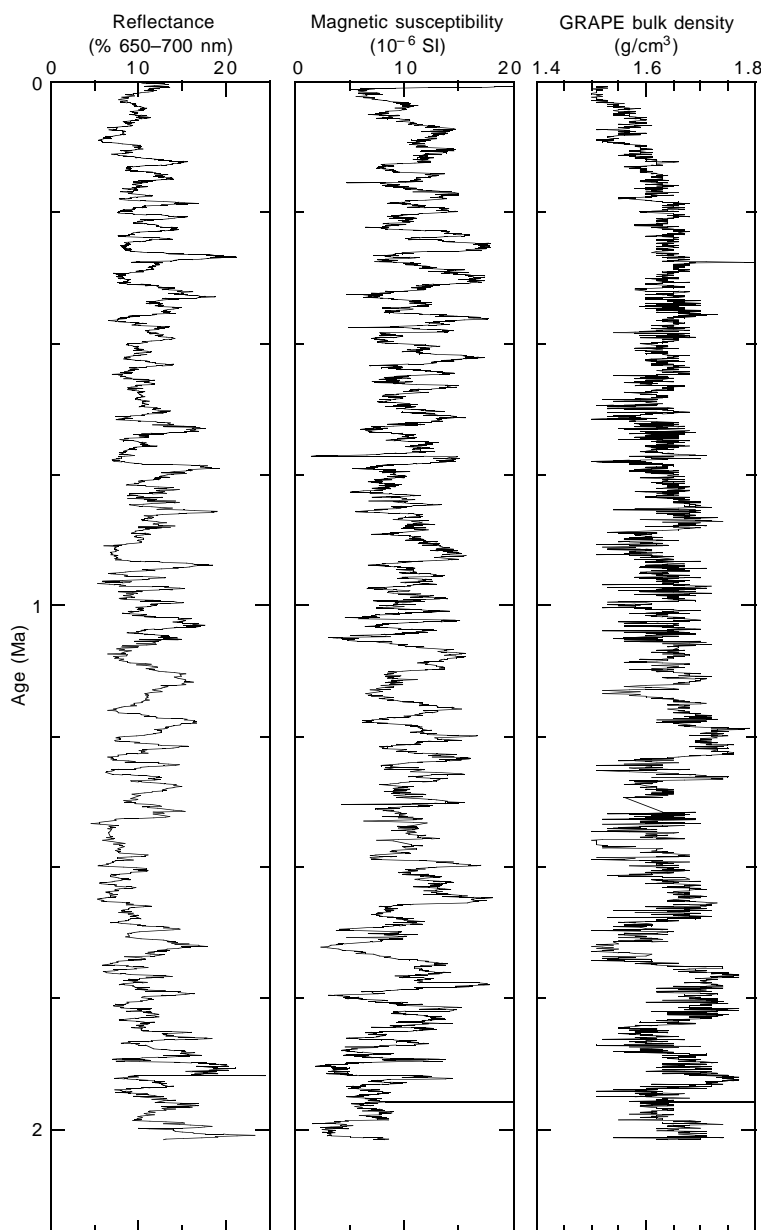


Figure 16. Spliced records of color reflectance, magnetic susceptibility, and GRAPE bulk density vs. age based on age control points from Table 11.

tion, this chapter), which caused very high attenuation of the signal that precluded measurements beyond Core 167-1012A-5H.

### Heat Flow

Thermal conductivity was measured in the sediment cores of Hole 1012B (Table 17 on CD-ROM in the back pocket of this volume) at an average of one per 3 m down to 98.55 mbsf. Four downhole temperature measurements were taken with the APC Adara temperature tool in Hole 1012B: 6.5°C at 37.3 mbsf, 7.9°C at 56.3 mbsf, 9.5°C at 75.3 mbsf, and 10.7°C at 94.3 mbsf in Cores 167-1012B-4H, 6H, 8H, and 10H, respectively (Fig. 25). The bottom-water temperature was measured during the Core 167-1012B-4H run, leaving the tool at the mudline for approximately 11.5 min before piston coring. The data indicate a bottom-water temperature of  $3.0^{\circ}\text{C} \pm 0.1^{\circ}\text{C}$ . The five data points yield a thermal gradient of  $82^{\circ}\text{C}/\text{km}$  (Fig. 26). Using an aver-

age measured thermal conductivity of  $0.905 \text{ W}/(\text{m}\cdot\text{K})$  provides a heat-flow estimate of  $74 \text{ mW}/\text{m}^2$  at Site 1012.

### Color Reflectance

Reflectance measurements in all holes at Site 1012 were taken at 4-cm intervals from 0 to 30 mbsf and at 6-cm intervals from 30 to 270 mbsf. Color reflectance values average 10%–15%, slightly higher than at Site 1011. To predict calcium carbonate at Site 1012, we used a multiple linear regression equation developed using calcium carbonate and reflectance measurements gathered at Site 1011. The color reflectance data were prepared for the regression by division into seventy 10-nm block-averaged bands, each representing brightness in their particular portion of the 250- to 950-nm spectrum. To quantify spectral shape, we took the first derivative of each block average, for a total of 140 independent variables. These independent variables

**Table 12. Interstitial water geochemical data, Hole 1012A.**

Core, section, interval (cm)	Depth (mbsf)	pH	Alkalinity (mM)	Salinity	Cl <sup>-</sup> (mM)	Na <sup>+</sup> (mM)	SO <sub>4</sub> <sup>2-</sup> (mM)	HPO <sub>4</sub> <sup>2-</sup> (μM)	NH <sub>4</sub> <sup>+</sup> (mM)	H <sub>4</sub> SiO <sub>4</sub> (μM)	Ca <sup>2+</sup> (mM)	Mg <sup>2+</sup> (mM)	Sr <sup>2+</sup> (μM)	Li <sup>+</sup> (μM)	K <sup>+</sup> (mM)
167-1012A-															
1H-2, 145-150	2.95	7.55	4.01	34.0	549	475	27.6	12	0.4	407	10.0	51.3	84	27	10.4
2H-3, 145-150	9.15	7.63	18.4	34.0	554	479	16.1	59	2.0	602	6.87	50.5	89	30	10.9
3H-3, 145-150	18.65	7.45	37.3	33.0	557	481	0.7	96	3.8	685	3.32	48.3	104	31	11.3
4H-3, 145-150	28.15	7.57	40.4	33.0	551	480	<0.7	123	5.0	814	2.88	47.1	132	36	11.7
5H-3, 145-150	37.65	7.42	43.4	33.0	551	483	<0.7	105	6.4	748	2.99	47.0	134	45	11.0
6H-3, 145-150	47.22	7.94	38.7	33.0	564	482	<0.7	91	11.0	674	2.16	45.7	112	58	
9H-3, 145-150	75.65	7.30	56.7	34.0	551	490	<0.7	93	11.1	956	3.58	49.3	177	110	11.7
12H-3, 145-150	104.32	7.48	62.7	35.0	550	492	<0.7	57	13.6	909	4.08	50.2	214	152	12.5
15X-2, 145-150	131.35	7.19	65.6	35.0	549	492	<0.7	79	14.9	1053	4.52	50.4	257	180	13.2
18X-3, 145-150	161.65	7.65	67.3	35.0	544	491	<0.7	56	15.9	1094	4.74	49.2	282	203	12.0
21X-4, 145-150	184.45	7.64	62.8	38.0	547	497	<0.7	28	14.4	1109	5.30	45.1	291	228	11.9
24X-3, 145-150	211.75	7.09	54.5	33.5	546	496	<0.7	23	14.5	1066	6.04	40.7	273	226	11.3
27X-3, 145-150	240.45	7.05	54.2	34.0	542	495	<0.7	27	15.1	1254	6.31	37.9	318	248	13.0
30X-3, 145-150	267.13	6.84	53.3	33.5	538	494	<0.7	16	15.2	1212	6.10	36.6	343	268	12.0

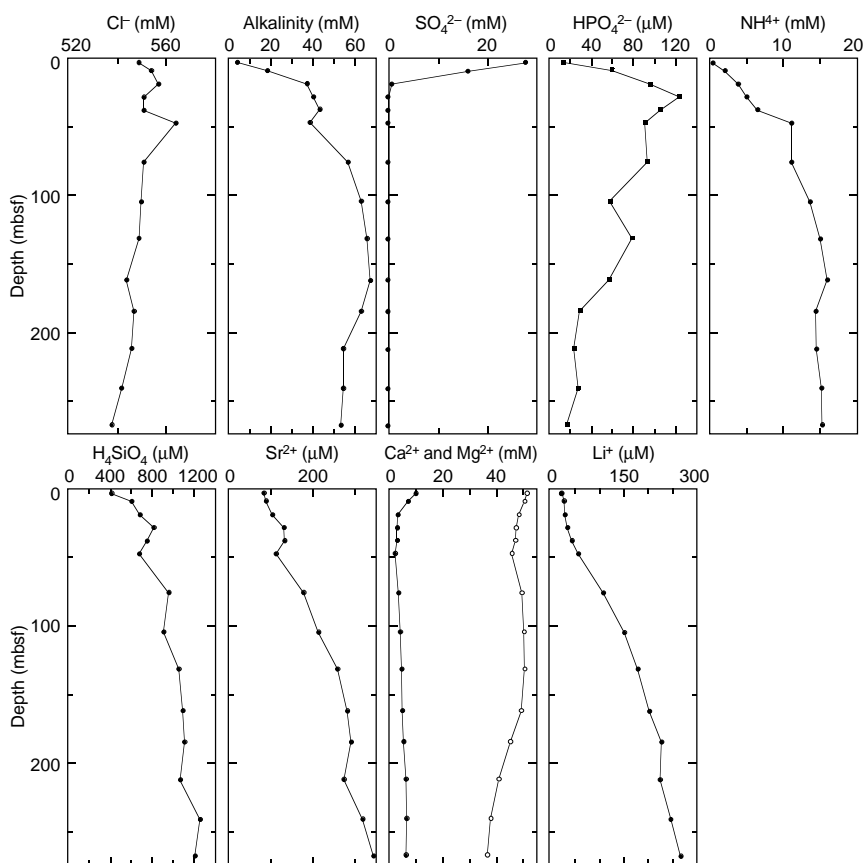


Figure 17. Interstitial water geochemical data, Site 1012. Solid circles = Ca, open circles = Mg.

were then regressed against the dependent variable, in this case calcium carbonate, using a step-wise regression technique. For Site 1011, the regression explained 87% of the observed calcium carbonate variability ( $r^2 = 0.87$ ).

A summary of measured Site 1012 calcium carbonate values and estimated values based on the Site 1011 regression equation is given in Figure 27. In general, the predicted signal matched the phase and amplitude of the actual values, though carbonate values are underestimated in some intervals. The high-resolution color reflectance data predict calcite variations not resolved by the low-resolution (one sample per 1.5 m) shipboard calcium carbonate measurements. These preliminary results demonstrate that reflectance may be a useful tool for high-resolution predictions of sedimentary calcium carbonate content.

**Digital Color Video**

Cores from Holes 1012A and 1012B were imaged with the ODP color digital imaging system over 20-cm intervals, providing a 0.25-mm pixel. There appears to be a good correlation of color data between the two holes (Fig. 28). CIELAB L\* values also correlate well with color reflectance data in the 450–500-nm band gathered by the Oregon State University (OSU) color reflectance tool (Fig. 29), although CIELAB a\* and b\* do not show a similar correlation. A good correlation of the intensity of color CIELAB L\* (see “Explanatory Notes” chapter, this volume) with discrete gravimetric bulk density is also seen, probably reflecting variations in calcium carbonate content (Fig. 30).

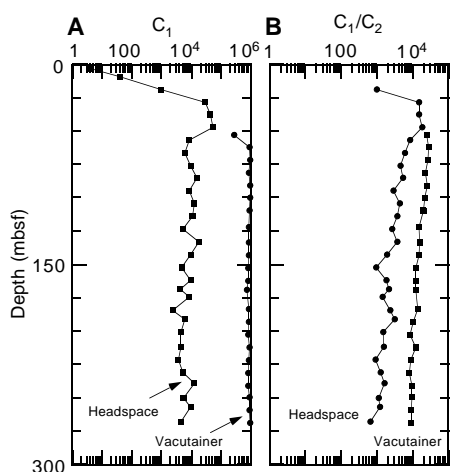


Figure 18. **A.** Concentrations of methane ( $C_1$ ) in ppm obtained by the headspace technique from Hole 1012A. **B.** Methane/ethane ratios of headspace and vacutainer measurements from Hole 1012A.

### SUMMARY

At Site 1012, in the East Cortes Basin of the California Borderland, we drilled a 273-m-thick high-resolution Neogene sedimentary section to upper Miocene sediments. The deepest hole reached roughly halfway through the sedimentary section in the basin (Fig. 31). Even though Site 1012 is in a water depth of 1783 mbsl, intermediate waters that fill the basin come from the basin sill depth of 1415 mbsl. The sediment column was triple cored to a depth of 86.9 mbsf (~1.2 Ma) and double cored to 132.3 mbsf (~2.0 Ma). A continuous spliced section could be verified only through the triple-cored section. Excellent magnetostratigraphy, with relatively strong magnetic intensity, was obtained through the APC-cored section (132.3 mbsf) despite relatively high organic carbon contents averaging ~2%–3% and active methanogenesis in the sediment column. The magnetic carrier phase has not yet been identified. In addition, good biostratig-

raphy was obtained through calcareous foraminifers and nannofossils. Radiolarians and diatoms are absent in the section.

Distinctive features to note within the lithostratigraphic column are the lack of siliceous microfossils at the site, except for prominent, reworked middle Miocene forms, and the high calcium carbonate content in the Pliocene section, which decreases by over half in the upper Pleistocene sediments. Diagenetic dolostones and high but variable calcium carbonate content appear to produce the strong reflectors in the seismic section, instead of variable deposition of diatomaceous sediments, which produced the strong reflections at Site 1011.

### REFERENCES

- Bordovskiy, O.K., 1965. Accumulation and transformation of organic substances in marine sediment, 2. Sources of organic matter in marine basins. *Mar. Geol.*, 3:5–31.
- Cande, S.C., and Kent, D.V., 1995. Revised calibration of the geomagnetic polarity timescale for the Late Cretaceous and Cenozoic. *J. Geophys. Res.*, 100:6093–6095.
- Emerson, S., and Hedges, J.I., 1988. Processes controlling the organic carbon content of open ocean sediments. *Paleoceanography*, 3:621–634.
- Emery, K.O., 1960. *The Sea off Southern California: a Modern Habitat of Petroleum*. New York (Wiley).
- Haq, B.U., Hardenbol, J., and Vail, P.R., 1987. Chronology of fluctuating sea levels since the Triassic. *Science*, 235:1156–1167.
- Lyle, M., Gallaway, P.J., Liberty, L.M., Mix, A., Stott, L., Hammond, D., Gardner, J., Dean, W., and the EW9504 Scientific Party, 1995a. Data submission. W9406 and EW9504 site surveys of the California margin proposed drillsites, Leg 167 (Vol. 1): Site maps and descriptions. Boise State Univ., *CGISS Tech. Rep.*, 95–11.
- Lyle, M., Gallaway, P.J., Liberty, L.M., Mix, A., Stott, L., Hammond, D., Gardner, J., Dean, W., and the EW9504 Scientific Party, 1995b. Data submission. W9406 and EW9504 site surveys of the California margin proposed drillsites, Leg 167 (Vol. 2): Seismic profiles. Boise State Univ., *CGISS Tech. Rep.*, 95–12.
- McCrory, P.A., Wilson, D.S., Ingle, J.C., Jr., and Stanley, R.G., 1995. Neogene geohistory analysis of Santa Maria Basin, California, and its relationship to transfer of central California to the Pacific Plate. In Keller, M.A. (Ed.), *Evolution of Sedimentary Basins/Onshore Oil and Gas Investigations—Santa Maria Province*. U.S. Geol. Surv. Bull., J1–J38.

Ms 167IR-106

**NOTE: For all sites drilled, core-description forms (“barrel sheets”) and core photographs can be found in Section 3, beginning on page 499. Smear-slide data can be found in Section 4, beginning on page 1327. Thin section data can be found in Section 5, beginning on page 1375. See Table of Contents for material contained on CD-ROM.**

**Table 13. Concentrations of methane (C<sub>1</sub>), ethene (C<sub>2=</sub>), ethane (C<sub>2</sub>), propene (C<sub>3=</sub>), propane (C<sub>3</sub>), isobutane (i-C<sub>4</sub>), n-butane (n-C<sub>4</sub>), isopentane (i-C<sub>5</sub>), n-pentane (n-C<sub>5</sub>) obtained by the headspace (Hole 1012A) and vacutainer techniques (various holes).**

Core, section, interval (cm)	Depth (mbsf)	C <sub>1</sub> (ppm)	C <sub>2=</sub> (ppm)	C <sub>2</sub> (ppm)	C <sub>3=</sub> (ppm)	C <sub>3</sub> (ppm)	i-C <sub>4</sub> (ppm)	n-C <sub>4</sub> (ppm)	i-C <sub>5</sub> (ppm)	n-C <sub>5</sub> (ppm)	C <sub>1</sub> /C <sub>2</sub>	C <sub>1</sub> /C <sub>3</sub>
Headspace												
167-1012A-												
1H-3, 0-5	3.03	4										
2H-4, 0-5	9.23	42										
3H-4, 0-5	18.73	1,000		1							1,000	
4H-4, 0-5	28.23	29,895		2							14,948	
5H-4, 0-5	37.73	46,074		3							15,358	
6H-4, 0-5	47.23	54,899		3							18,300	
7H-4, 0-5	56.73	8,555		1							8,555	
8H-4, 0-5	66.23	6,133		1							6,133	
9H-4, 0-5	75.73	9,361		2							4,681	
10H-4, 0-5	85.23	15,992	1	3							5,331	
11H-4, 0-5	94.73	8,697	1	3		1					2,899	8,697
12H-4, 0-5	104.23	12,952	1	3		1					4,317	12,952
13H-4, 0-5	113.73	11,032	1	3		2					3,677	5,516
14X-4, 0-5	123.23	5,457		2		1					2,729	5,457
15X-3, 0-5	131.43	18,928	1	5		4					3,786	4,732
16X-4, 0-5	142.53	9,539	1	5		5					1,908	1,908
17X-4, 0-5	152.13	4,740	1	5		5					948	948
18X-4, 0-5	161.73	9,382	1	5		5					1,876	1,876
19X-2, 0-5	168.33	4,444		2		1					2,222	4,444
20X-4, 0-5	174.43	8,797	1	6		8					1,466	1,100
21X-5, 0-5	184.53	2,400		1							2,400	
22X-3, 0-5	191.03	6,236		2		3					3,118	2,079
23X-3, 0-5	200.63	4,580	1	3		3					1,527	1,527
24X-4, 0-5	211.83	4,626	7	3		3					1,542	1,542
25X-3, 145-150	221.18	3,686		4		6					922	614
26X-4, 0-5	230.93	5,190		4		5					1,298	1,038
27X-2, 145-150	238.98	12,948	1	8		10					1,619	1,295
28X-3, 145-150	249.88	5,683	7	5		6					1,137	947
29X-2, 145-150	256.98	9,697	2	8		10					1,212	970
30X-4, 0-5	267.83	4,587	2	7		8					655	573
Vacutainer												
167-1012A-												
7H-1, 50-51	52.71	277,760		11		3					25,251	92,587
8H-1, 50-51	62.21	928,111		33		7					28,125	132,587
9H-1, 50-51	71.71	941,984		34		8					27,705	117,748
10H-1, 50-51	81.21	876,234		38		10					23,059	87,623
11H-1, 50-51	90.71	958,346		37		8					259,011	19,793
12H-1, 50-51	100.21	942,000		43		11					21,907	85,636
13H-1, 50-51	109.71	932,013		47		14					19,830	66,572
14X-3, 50-51	122.21	853,044		56		16					15,233	53,315
167-1013A-												
15X-4, 50-51	133.41	877,485		56		16					15,669	54,843
167-1014A-												
16X-4, 50-51	143.01	864,915		57		17					15,174	50,877
167-1015A-												
17X-4, 50-51	152.61	849,801		67		22					12,684	38,627
167-1016A-												
18X-4, 50-51	162.21	850,176		69		147	14	17			12,321	5,784
167-1017A-												
19X-2, 50-51	168.81	773,476		61		21	13				12,680	36,832
167-1018A-												
21X-4, 50-51	183.51	856,171		62		23	18	17			13,809	37,225
167-1019A-												
22X-4, 50-51	193.01	851,969		82		36	29	17	24	17	10,390	23,666
167-1020A-												
23X-4, 50-51	202.61	820,246		98		46	34	19	29	17	8,370	17,831
167-1021A-												
24X-4, 50-51	212.31	897,797		73		29	27	15	22	17	12,299	30,959
167-1022A-												
25X-4, 50-51	221.71	874,767		97		41	33	18	25	17	9,018	21,336
26X-4, 50-51	231.41	833,428		103		42					8,092	19,844
27X-4, 50-51	241.01	851,002		87		32					9,782	26,594
28X-4, 50-51	249.61	921,670		94		32					9,805	28,802
29X-4, 50-51	259.21	909,101		100		33					9,091	27,549
30X-4, 50-51	268.91	958,456		103		25					9,305	38,338

**Table 14. Depth variations in concentrations of inorganic carbon, calcium carbonate, total carbon, total organic carbon, total nitrogen, and total sulfur in weight percent (wt%) in Hole 1012A.**

Core, section, interval (cm)	Depth (mbsf)	Inorganic carbon (wt%)	CaCO <sub>3</sub> (wt%)	Total carbon (wt%)	Total organic carbon (wt%)	Total nitrogen (wt%)	Total sulfur (wt%)	Total organic carbon/total nitrogen	Total organic carbon/total sulfur
167-1012A-									
1H-1, 29-30	0.29	3.61	30.1	6.68	3.07	0.38	0	8.08	
1H-2, 29-30	1.79	2.89	24.1	6.14	3.25	0.35	0	9.29	
1H-2, 29-30	1.79	2.38	19.8	5.39	3.01	0.33	0.99	9.12	3.04
2H-1, 29-30	4.99	2.32	19.3	5.64	3.32	0.37	0	8.97	
2H-2, 29-30	6.49	1.34	11.2	5.82	4.48	0.48	0.99	9.33	4.53
2H-3, 29-30	7.99	0.84	7	7.33	6.49	0.66	1.02	9.83	6.36
2H-4, 29-30	9.49	1.15	9.6	4.3	3.15	0.33	0.6	9.55	5.25
2H-5, 29-30	10.99	2.46	20.5	4.02	1.56	0.19	0.43	8.21	3.63
2H-6, 29-30	12.49	3.73	31.1	6.52	2.79	0.28	0.32	9.96	8.72
2H-7, 29-30	13.99	3.59	29.9	5.53	1.94	0.22	0	8.82	

Only part of this table is produced here. The entire table appears on CD-ROM, back pocket, this volume.

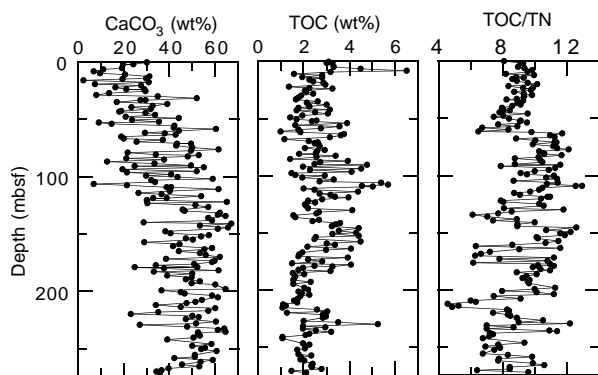


Figure 19. Calcium carbonate and organic carbon data in weight percent (wt%) and TOC/TN vs. depth (mbsf) from sediments of Hole 1012A.

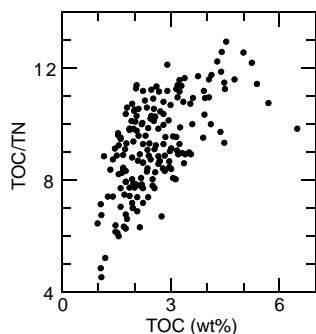


Figure 20. Total organic carbon (TOC) content vs. total organic carbon/total nitrogen (TOC/TN) in sediments of Hole 1012A.

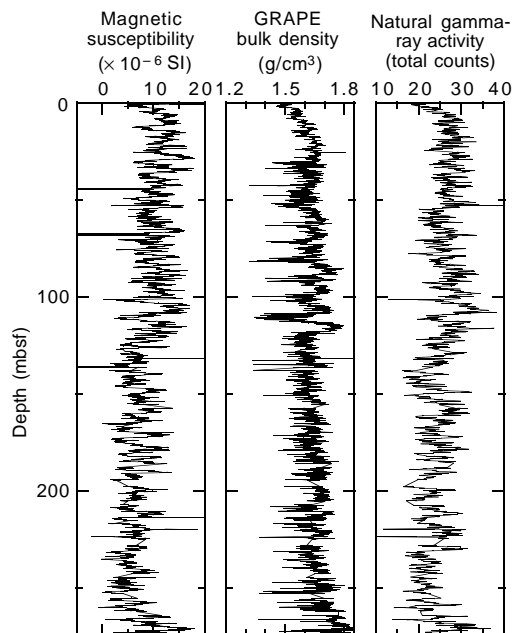


Figure 21. MST data from Hole 1012A.

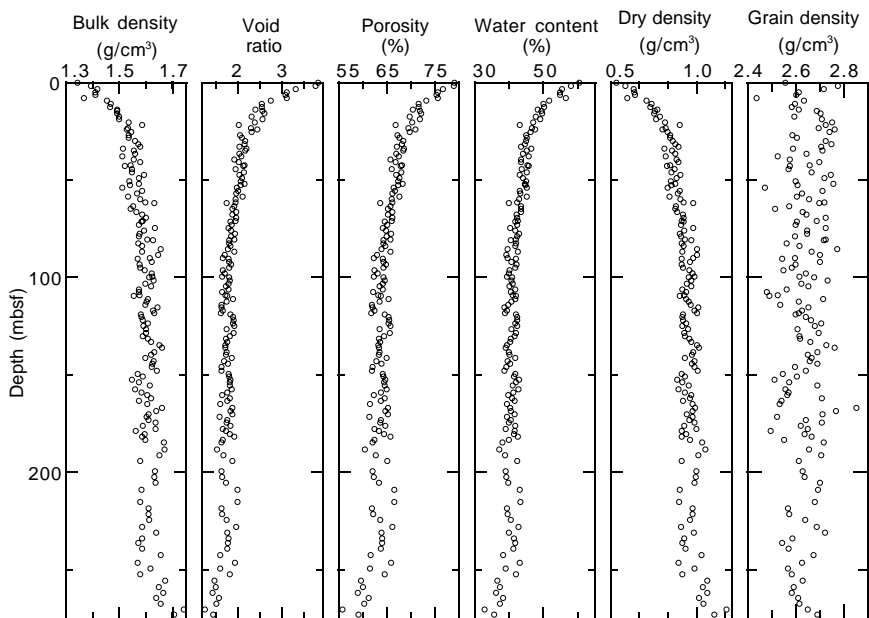


Figure 22. Index properties data from Hole 1012A.

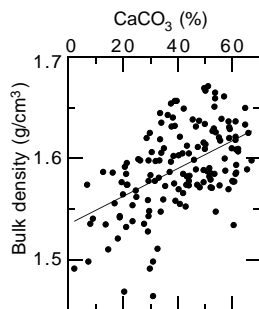


Figure 23. Gravimetric bulk density vs. discrete calcium carbonate content from Hole 1012A with best-fit line from least-squares linear regression.

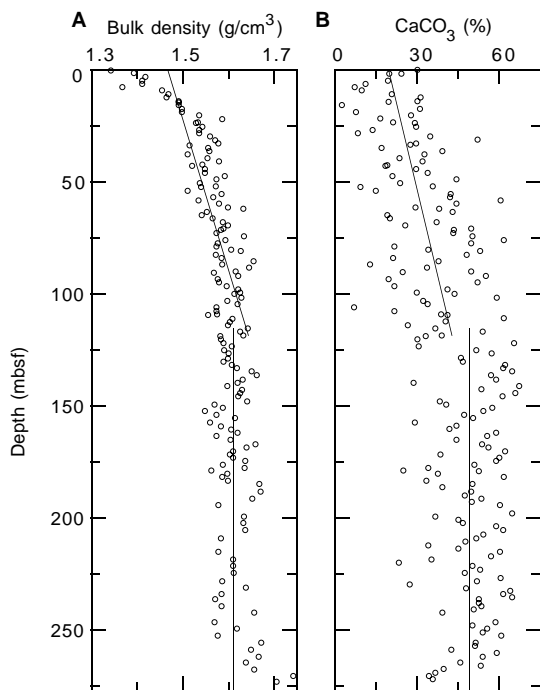


Figure 24. **A.** Hole 1012A gravimetric bulk density. **B.** Hole 1012A discrete calcium carbonate content data. Both properties increase downhole.

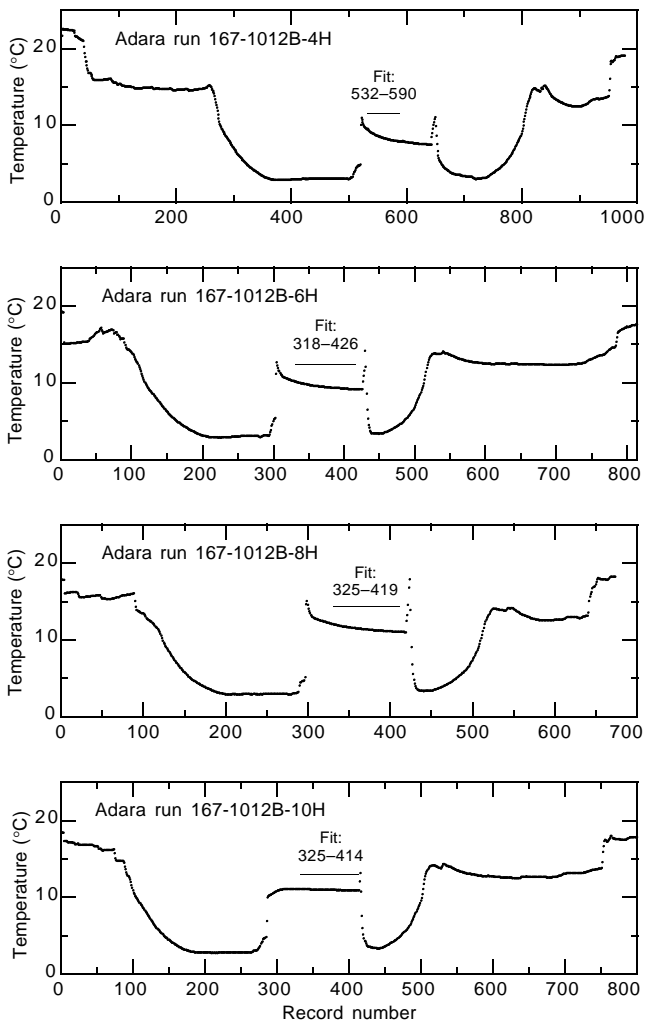


Figure 25. Hole 1012B downhole temperature vs. record number (5-s recording frequency) for each measurement run, showing interval fitted to determine downhole temperature.

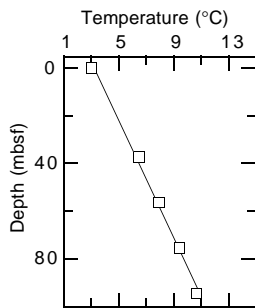


Figure 26. Downhole temperature gradient for Hole 1012B.

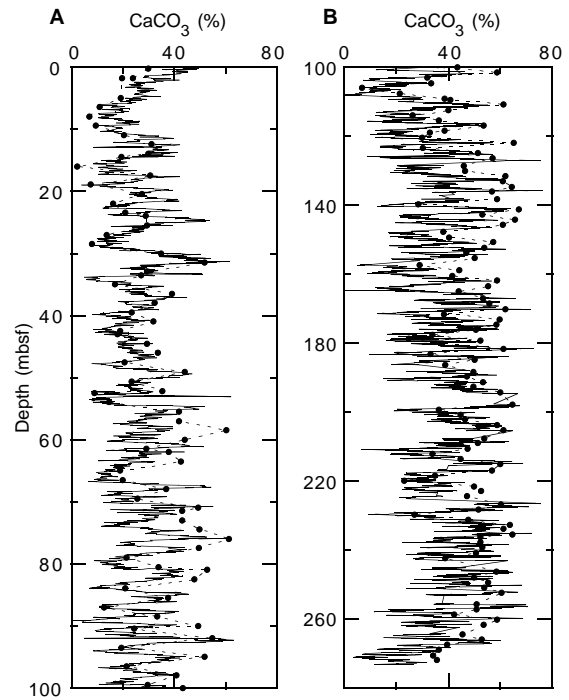


Figure 27. Summary of measured (dashed line joining dots) and estimated calcium carbonate values (solid line) for (A) 0–100 mbsf and (B) 100–280 mbsf at Hole 1012A.

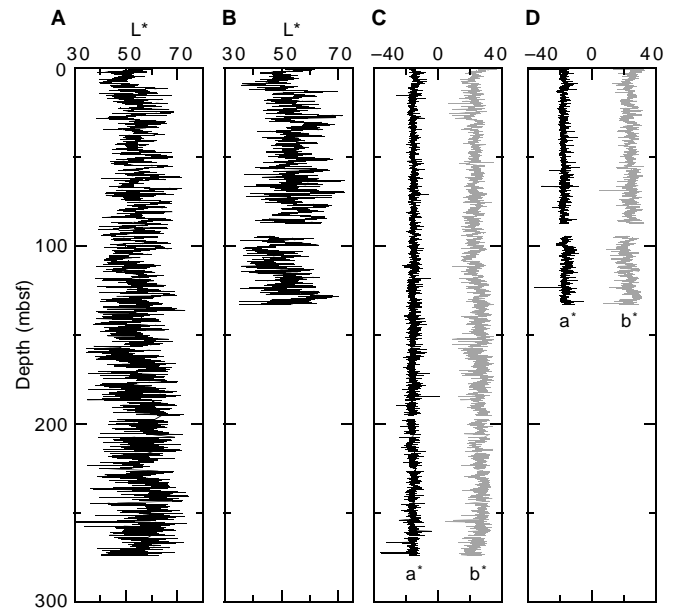


Figure 28. A and B. Intensity of color CIELAB  $L^*$  vs. depth plots for Holes 1012A and 1012B, respectively. C and D. CIELAB  $a^*$  and  $b^*$  vs. depth plots for Holes 1012A and 1012B, respectively.

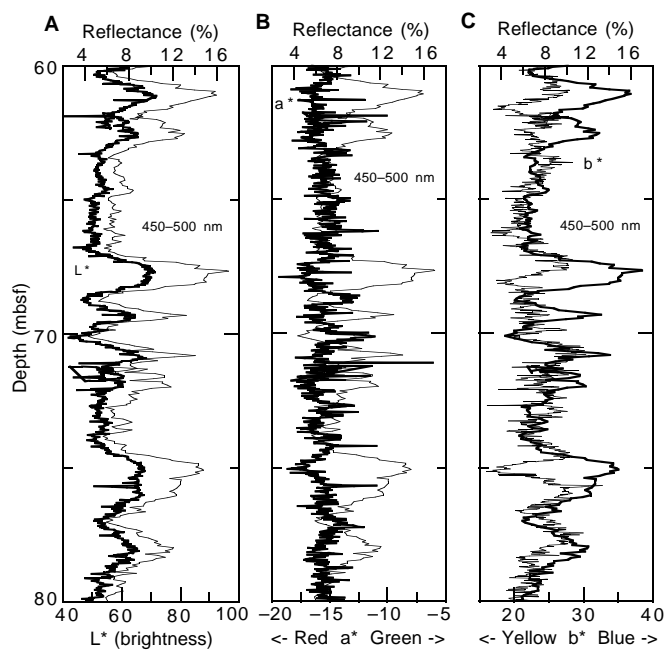


Figure 29. Comparison of Hole 1012A color reflectance values measured by the ODP color digital imaging system (thick line) to color reflectance values (450- to 500-nm band) obtained by the OSU multiwavelength color reflectance tool (thin line). **A.** CIELAB L\*. **B.** CIELAB a\*. **C.** CIELAB b\*. There are peaks in CIELAB L\* corresponding to reflectance peaks. However, the relationships between color reflectance and CIELAB a\* and b\* values are less clear.

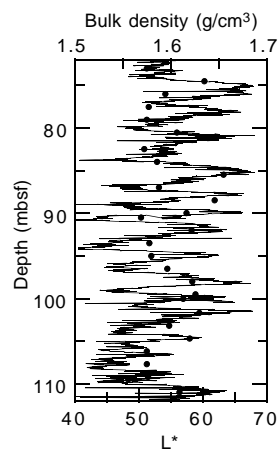


Figure 30. Intensity of color CIELAB L\* from the digital color video (line) and gravimetric bulk density (dots). CIELAB L\* data are decimated at 2-cm intervals.

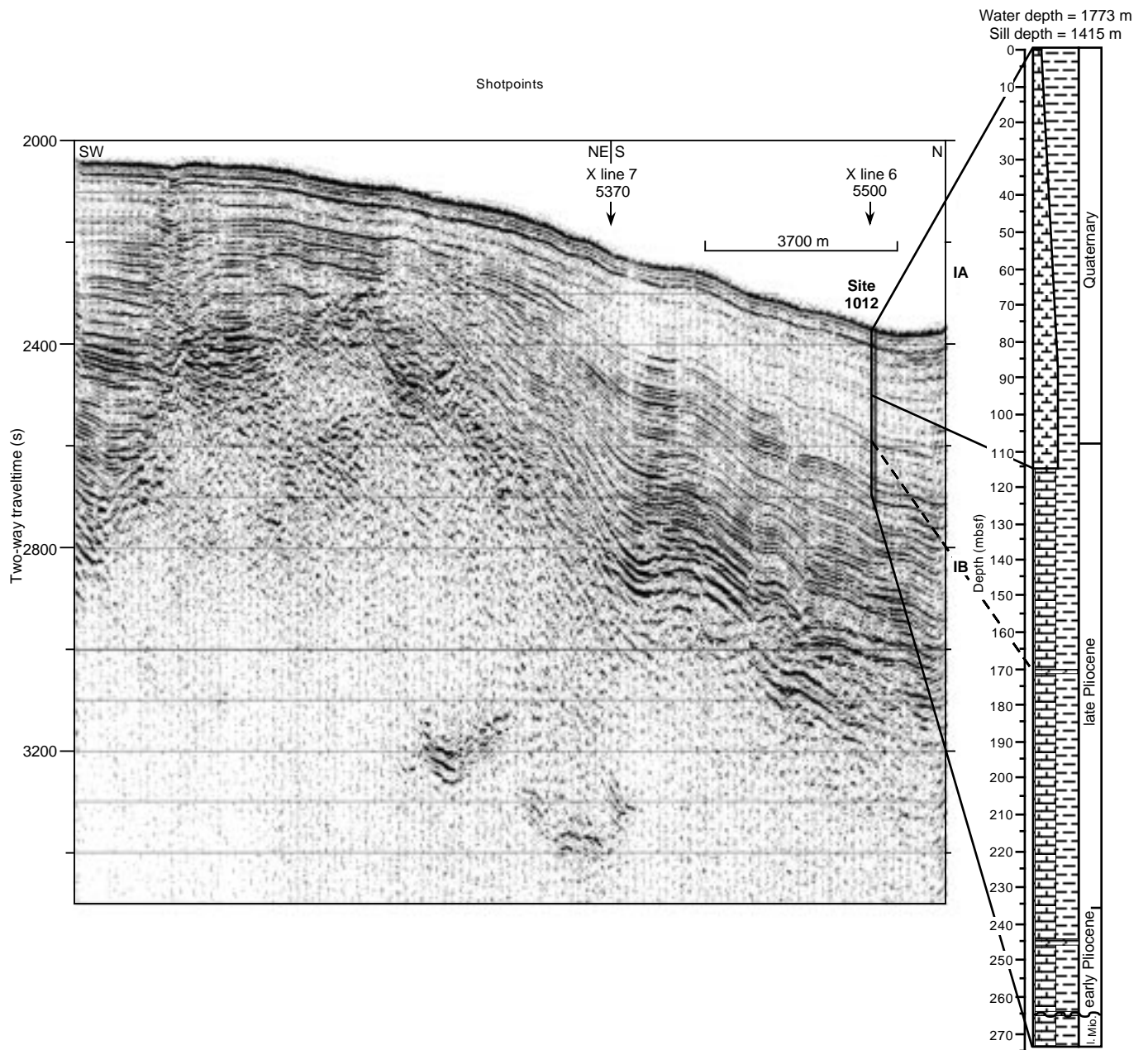


Figure 31. Comparison of the lithostratigraphic column at Site 1012 and a seismic profile through the site (Lines EW9504 BA1-8 to 10; Lyle et al., 1995a, 1995b). Ties are calculated from measured seismic velocities (see “Physical Properties” section, this chapter). On y-axis, (s) = milliseconds.